

# The evolution of depletion zones beneath mud volcanoes

Joe Cartwright<sup>a,\*</sup>, Chris Kirkham<sup>a</sup>, D. Nicolas Espinoza<sup>b</sup>, David James<sup>c</sup>, Neil Hodgson<sup>d</sup>

<sup>a</sup> Department of Earth Sciences, University of Oxford, OX1 3AN, UK

<sup>b</sup> Department of Petroleum Engineering and Geosystems Engineering, The University of Texas at Austin, Austin, TX, USA

<sup>c</sup> Cwmystwyth, Ceredigion, Wales, UK

<sup>d</sup> Searcher Geodata Ltd, Unit 6, Albion House, High St, Woking, GU21 6BG, UK

## ARTICLE INFO

### Keywords:

Mud volcano  
Depletion zones  
Liquefaction  
Overpressure  
Hydraulic fracturing

## ABSTRACT

Depletion zones are the least well understood component of mud volcanic systems. They are generally difficult to image using reflection seismic data, and have only rarely been identified and described in the subsurface. This study documents 277 mapped depletion zones in the western Nile Cone, offshore Egypt, of which the dimensions and stratigraphic characteristics of a sub-set of 86 depletion zones associated with mud volcanoes of early Pliocene to Recent age are recorded. The primary database used is a large (4,300 km<sup>2</sup>) 3D seismic survey in which depletion zones can be confidently interpreted using a set of simple criteria. The sub-set of 86 depletion zones were selected for morphometric analysis by virtue of the quality of seismic imaging. The depletion zones are characterised by circular to elliptical planforms with a bowl or conical geometry. They exhibit truncational stratal relationships with their parent stratigraphic unit, which in this area is the Mid-Late Miocene aged OM2 unit, and which occurs directly beneath the Messinian Evaporites. This geometry implies a top-down formation mechanism. Their diameters and relief range from 600 m–3300 m, and 100 m–740 m, respectively, with a modest scaling relationship between diameter and relief. Flank angles of bowls and cones range from 11° to 41°, with a crudely normal distribution, with median and mean values of 26°. A model for the evolution of depletion zones in the study area is based on two previous models developed for single source layer plumbing systems and invokes mobilisation of the source layer by sediment collapse and shear-induced liquefaction following initial seal failure by hydraulic fracturing of the evaporite seal. This mechanism may be more widely applicable to mud volcano systems than currently appreciated.

## 1. Introduction

Mud volcanoes are widely distributed in a range of tectonic settings (Milkov, 2000; Mazzini and Etiope, 2017) and are important to understand not least because they represent a significant natural venting locus for methane emissions to the atmosphere (Etiope and Klusman, 2002). On rare occasions they also represent a significant geohazard (Davies et al., 2008; Deville and Guerlais, 2009). In spite of extensive research into their genesis in recent decades (see reviews in Kopf, 2002; Dimitrov, 2002; Mazzini and Etiope, 2017), there is still considerable uncertainty over the precise mechanisms by which muddy materials are mobilised at depth and transported to the surface. This deeper part of the mud volcanic ‘plumbing system’ is rarely exposed at surface, and our understanding relies on indirect inferences made from the extruded products or by more direct observation by seismic imaging.

The plumbing system of mud volcanoes comprises the conduits along

which muddy slurry is transported and the intervals from which the mud and component fluids are primarily derived or stored en route (Dupuis et al., 2019). Indirect methods for identifying the source regions or parent beds for the volcano rely on an analysis of the clasts transported and ejected in the muddy slurry (e.g. Deville et al., 2003; Praeg et al., 2009) or geochemical fingerprinting of the fluids in the slurry (Planke et al., 2003). More direct methods are based on seismic imaging of the stratigraphic intervals where depletion of parental fine-grained sediments have been mobilised and transported to the surface (Graue, 2000; Stewart and Davies, 2006; Kirkham et al., 2017; Dupuis et al., 2019).

These contrasting methods have been applied to a variety of mud volcanoes from different geological settings and unsurprisingly have led to contrasting ideas on how mud volcanoes are fed, broadly subdivided into two main categories (Fig. 1) (Dupuis et al., 2019). The first is a multi-layered sourcing model, in which sourcing of mud and fluids occurs from a number of stratigraphic units over a substantial depth range.

\* Corresponding author.

E-mail address: [joec@earth.ox.ac.uk](mailto:joec@earth.ox.ac.uk) (J. Cartwright).

<https://doi.org/10.1016/j.marpetgeo.2023.106351>

Received 5 April 2023; Received in revised form 31 May 2023; Accepted 1 June 2023

Available online 10 June 2023

0264-8172/© 2023 The Authors. Published by Elsevier Ltd. This is an open access article under the CC BY-NC-ND license (<http://creativecommons.org/licenses/by-nc-nd/4.0/>).

This may or may not include storage of mud in chambers at some point in the upwards transport path, and the cannibalisation of early extruded material to form later extrusions (Fig. 1A). The second category is based mainly on use of seismic data, and in contrast invokes mobilisation of the bulk of the extruded volume from a single stratigraphic ‘source’ or ‘parent’ layer. Once this mobilised volume has been transported to the surface it leaves behind a recognisable subsurface structure referred to as a depletion zone (Fig. 1B).

Depletion zones have been identified and described in only a limited number of cases to date, primarily because high fidelity 3D seismic imaging of these structures is only rarely achieved. The first study that used 3D seismic reflection data to identify depletion zones and quantify the volume of depleted mud was by Graue (2000) for a suite of mud volcanoes from offshore Nigeria. Stewart and Davies (2006) later presented a full 3D visualisation of the source region underlying a mud volcano in the Caspian Sea and were the first to coin the term “depletion zone” as part of the mud volcano system. Kirkham et al. (2017) used high resolution 3D data from a mud volcano province offshore Egypt, to identify and quantify the depleted and extruded volumes. Dupuis et al. (2019) identified multiple episodes of roof collapse during mud depletion and the eruption of stacked mud volcanoes offshore Nigeria. These authors introduced the term “mud weld” to describe the surface resulting from progressive collapse of the roof of a mud source unit following depletion.

Kirkham et al. (2017) and Dupuis et al. (2019) both presented qualitative models for depletion zone evolution. Common to both is an episodic liquefaction mechanism by which the depletion zone grows in a ‘top down’ geometrical evolution, with mobilisation of a parent layer both outwards and downwards from an initial locus. The proposed conditions for liquefaction in these two models differ considerably, with Kirkham et al. (2017) favouring propagation by progressive collapse of the intact parent material into a slurry-filled chamber at the base of the conduit. They suggested that this process was analogous to that responsible for some quick clay mobilisation phenomena. In contrast, Dupuis et al. (2019) argue for mobilisation via a gas exsolution and expansion process, with a locus related to zones of upward gas accumulation.

These qualitative models for depletion zone evolution offer relatively simple alternatives to the more complex and widely held view that mud volcanoes have polygenetic sources and where the mobilisation of the muddy slurry is intrinsically linked to the upwards focused flow of

deeply sourced fluids (Deville et al., 2010). However, because so few depletion zones have been described in detail, it is not possible to generalise the conditions for their formation and to examine the extent to which this single source layer model may be more generally applicable.

The aim of this paper, therefore, is to further evaluate the generalised concept of top down liquefaction by focusing on detailed quantification of depletion zone geometry from a single well imaged mud volcano province. We present a comprehensive set of measurements of depletion zones at various stages in their evolutionary history and analyse these to evaluate the precise mechanism of liquefaction involved in their formation. In particular, we draw on the previous approaches of Kirkham et al. (2017) and Dupuis et al. (2019) in linking the depletion zone geometry to their extruded counterpart, and examine the subsidence of the overburden and internal geometry of the surface edifice to the depleted source layer in conjunction with the depletion zone itself. It is hoped that by furthering our understanding of depletion zone evolution, we can help stimulate additional investigations of this important, but hitherto relatively neglected aspect of mud volcanism.

## 2. Geological setting

### 2.1. Geodynamic evolution and structural regime

The study area is located within the lower slope region of the west Nile Deep Sea Fan (Fig. 2A & B). This large sedimentary cone was deposited on the passive margin formed by rifting of a broader region of the Eastern Mediterranean during the Jurassic-Early Cretaceous (Salem, 1976; Dolson et al., 2005). Carbonates were deposited over much of the North African margin through the Late Cretaceous-Mid Eocene, until uplift of East Africa led to an increase in northerly drainage and a switch to clastic deposition in the Mid-Late Eocene (Underwood et al., 2013). From the Late-Eocene to the Late Miocene, the basin fill was dominated by marine shales, confined turbidites and multi-story channel systems (Fig. 2C & D) (Kellner et al., 2018; Dolson, 2020; Abd El-Fattah et al., 2021). During the Late Miocene, the Mediterranean Sea became increasingly restricted from the Atlantic Ocean, leading to the Messinian Salinity Crisis (~5.97–5.33 Ma). This resulted in deposition of a 1–1.5 km thick evaporitic sequence (predominantly halite) over large parts of the Eastern Mediterranean (Fig. 2) (Hsü et al., 1977; Meilijson et al., 2019). Significant drawdown during the early stages of the Messinian

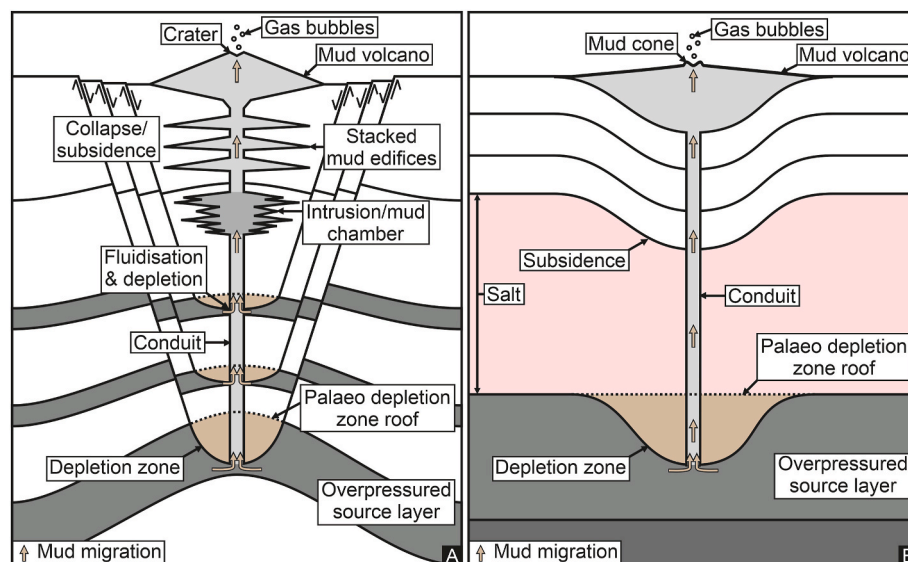
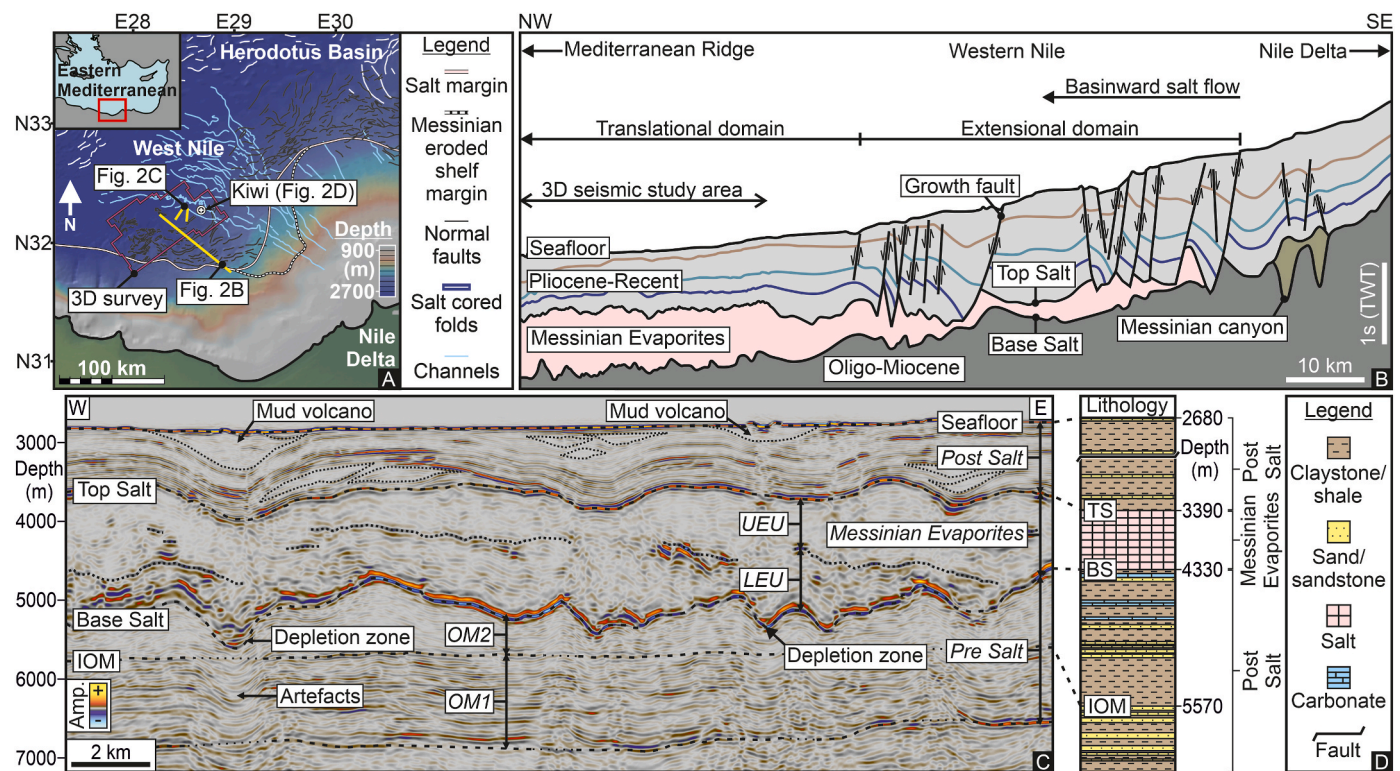


Fig. 1. Multi-layer and single layer depletion during mud volcanism. A: A model for multi-layer mud depletion (adapted from Planke et al., 2003, Deville et al., 2010 and Mazzini and Etiope, 2017) where mud is sourced from more than one stratigraphic unit. B: A model for single layer mud depletion (adapted from Kirkham et al., 2017) in which the bulk of the mud is remobilised from a single source unit.



**Fig. 2.** Geological setting of the west Nile Deep Sea Fan. **A:** A bathymetric map (from GeoMapApp [www.geomapp.org](http://www.geomapp.org)) of the west Nile Delta and west Nile Deep Sea Fan showing channels from the Rosetta branch of the Nile Delta, the margins of the salt basin (modified from Loncke et al., 2006 and Lofi et al., 2011), thin-skinned normal faults and salt cored anticlines (compiled from Allen et al., 2016; Loncke et al., 2006; Zucker et al., 2020 and Kirkham and Cartwright, 2022) and the location of the 3D seismic survey and Kiwi exploration well. **B:** A regional cross-section (see Fig. 2A for location; modified from Allen et al., 2016 and Kirkham et al., 2022) spanning NW-SE across the west Nile Delta and Nile Deep Sea Fan. **C:** A seismic cross-section in depth through the 3D seismic survey area (see Fig. 2A for location) showing the main seismic stratigraphic horizons and units, as well as mud volcanoes and depletion zones. IOM – Intra-Oligo-Miocene; OM – Oligo-Miocene; UEU – Upper Evaporitic Unit; LEU – Lower Evaporitic Unit. **D:** Lithological column from the Kiwi well (see Fig. 2A for location) in the 3D seismic survey area. TS – Top Salt; BS – Base Salt.

Salinity Crisis resulted in widespread erosion (Ryan, 2009). Up to >1000 m of Oligo-Miocene clastic sediments were excavated in the study area to form a series of canyons and ridges that are preserved at the base of the thick salt layer (Mousoulitis et al., 2020; Kirkham et al., 2022). Re-flooding of the Mediterranean during the Early Pliocene terminated evaporite deposition (Garcia-Castellanos et al., 2009) and renewed clastic deposition that has persisted to the present day and led to the development of the Nile Delta and Nile Deep Sea Fan (Fig. 2) (Loncke et al., 2006).

The basin is structurally controlled by a complex interaction of thick and thin-skinned tectonics. The NE-SW Rosetta Fault System and NW-SE Tensah Fault System are considered to be inherited from pre-existing basement structures that formed during the rifting (Aal et al., 2000; Abd El-Fattah et al., 2021). Thin-skinned gravity tectonics within the Messinian-Recent successions has overprinted much of the thick-skinned tectonics in the study area (Fig. 2A & B) (Loncke et al., 2006; Allen et al., 2016). Regional flow of the Messinian salt during the Pliocene-Recent has led the development of 1) an extensional domain characterised by a margin-parallel (NE-SW) belt of normal faults that detach in the salt, 2) a translational domain with few extensional or contractional structures and 3) a contractional domain dominated by salt cored anticlines and thrust faults that detach in the Messinian salt (Fig. 2A & B) (Allen et al., 2016; Kirkham and Cartwright, 2022). The study area straddles the extensional and translational domains (Fig. 2B). A general north-westerly (basinward) flow of salt commencing in the mid Pliocene with up to 7.5 km of translation of the post-salt sedimentary succession has been documented for this area (Kirkham and Cartwright, 2022). This basinward flow means that many of the older mud volcanoes have been displaced relative to their pre-salt depletion zones (see below).

This study focuses on the Oligocene to Recent stratigraphic interval. We follow Kirkham et al. (2017) in subdividing the stratigraphy into three main units for descriptive ease (Fig. 2C). The 'Pre Salt' is taken as the Oligo-Miocene succession up to the base of the Messinian evaporites. The 'Messinian Evaporites' are Late Miocene in age and are defined by the Base and Top Salt marker horizons. The 'Post Salt', encompasses the Pliocene to Recent clastic succession in which all the mud edifices are found. Seismic stratigraphic descriptions of these units are presented in the following sections.

## 2.2. Mud mobilisation in the Eastern Mediterranean

Mud volcanoes have been recognised in many sub-basins of the Eastern Mediterranean (Masclé et al., 2014) including the Mediterranean Ridge (Cita, 1981; Camerlenghi et al., 1995), Florence Rise (Woodside et al., 2002), South Levant Basin (Netzeband et al., 2006), Nile Delta and Nile Deep Sea Fan (Loncke et al., 2004; Dupré et al., 2007, 2014; Huguen et al., 2009). The study area in the west Nile Deep Sea Fan is unique in comparison to the other sub-basins in that it hosts one of the most densely populated mud volcano fields on Earth (Kirkham et al., 2017).

Mud volcanism has occurred in the west Nile Deep Sea Fan throughout the Pliocene to Recent, and a number of present-day mud volcanoes are known to be active (Huguen et al., 2009). Giant mud volcanoes and mud canopies that individually cover areas of up to c. 315 km<sup>2</sup> and have volumes of c. 116 km<sup>3</sup> were extruded directly over the Messinian Evaporites (Kirkham et al., 2018a, 2020b). In addition, approximately 400 smaller mud volcanoes have erupted throughout the Pliocene-Recent in the study area. They are sourced from the immediate



Pre Salt succession and are fed by pipe-like conduits that transect the regional evaporitic seal (Kirkham et al., 2018b) and root to depletion zones within the uppermost Pre Salt (Kirkham et al., 2017). These mud volcanoes are primarily composed of grey-blue mud and mud breccia containing kaolinite, an abundance of smectite and little to no illite, with some silty and sandy intervals (Giresse et al., 2010).

Recently extruded mud volcanoes are all vertically aligned with their conduit and depletion zone. However, basinward translation of the Post Salt during salt tectonic deformation has resulted in offset of palaeo mud volcanoes from above their respective depletion zones in the Pre Salt (Kirkham and Cartwright, 2022).

### 3. Data and methods

The primary dataset used for this study includes a pre-stack time migrated (PSTM) and pre-stack depth migrated (PSDM) three-dimensional (3D) seismic survey, both of which cover the same c. 4300 km<sup>2</sup> (Fig. 2A). The binset dimensions are 12.5 × 6.25 m and the lateral resolution is 25 m. The dominant frequency is 20 and 60 Hz, respectively in the immediate Pre Salt and Post Salt successions and the corresponding vertical resolutions are c. 40 m and 10 m. The data have been processed to zero-phase and are displayed in SEG normal polarity (Brown, 2004). A low signal-to-noise ratio, migration and transmission artefacts, multiples and converted wave interference patterns complicate the imaging in the pre-salt succession, particularly close to the base of the salt.

Key marker horizons of the Seafloor, Top Salt, Base Salt and Intra Oligo-Miocene (IOM) (Fig. 2C) were manually picked and auto correlated regionally using Schlumberger's seismic interpretation software package, Petrel. The upper, basal and internal reflections of mud edifices were mapped locally following the criteria established in Fowler et al. (2000) and Mazzini and Etiope (2017).

The dimensions of mud volcanoes, depletion zones and local subsidence depressions were recorded using the measuring tool within Petrel (Fig. 3). Errors in these measurements are limited to the vertical and horizontal resolution of the seismic data. The volume of the depletion zones was calculated by automatic volumetric computation between an interpolated surface representing the assumed position of the Base Salt prior to remobilisation and depletion and the actual Base Salt surface. The interpolation made use of the fact that the margins of depletion zones are defined by a hinge representing the thinning of the depleted layer and the roof subsidence into that zone of thinning (Fig. 3).

### 4. Results

#### 4.1. Seismic stratigraphy of the Pre Salt, Messinian Evaporites and Post Salt

The Pre Salt has a wedge-shape geometry that increases in thickness northward from 200 to 3000 m. Its base is defined by a regionally correlatable positive and high amplitude reflection that is interpreted as

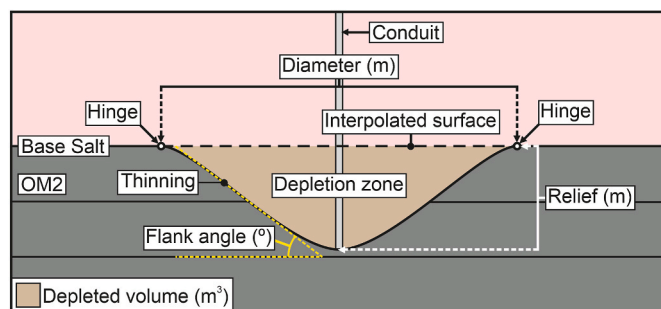


Fig. 3. A schematic of a depletion zone in the study area, showing the main features and measurements that can be extracted.

the boundary between carbonate ramp and clastic basin fill during the Upper Eocene (Kirkham et al., 2022). The Pre Salt is divided into two sub-units, Oligo-Miocene 1 (OM1) and Oligo-Miocene 2 (OM2), based on contrasts in seismic facies and unit geometry (Fig. 4).

OM1 is characterised by moderate amplitude and continuous stratal reflections. The reflections in OM1 dip gently basinward to the N-NE, are internally parallel and onlap onto the Eocene carbonate ramp (Fig. 4). OM1 is composed of marine shales and sandstones within stacked channel systems and basin floor fans (Fig. 4) (Kellner et al., 2018; Kirkham et al., 2022).

OM2 is characterised by much lower amplitude reflections than OM1 (Fig. 4). The boundary between OM1 and OM2 (IOM) is taken at this major seismic facies boundary. The internal reflection geometry is locally parallel, but there is a regional thickening northwards across the study area from 200 m to 1000 m. The lithology of OM2 is interpreted to be predominantly fine grained marine deposits. The lack of direct calibration means that both OM1 and OM2 are undated.

The Messinian Evaporites are defined by regionally continuous and mappable markers at top and base. The Top Salt is a high amplitude, positive reflection (Fig. 4), that can be easily mapped over the study area. It is generally concordant with the overlying early Pliocene clastic succession, except in localised areas of early mud extrusion. In contrast, the high amplitude negative reflection of the Base Salt is highly discordant to the underlying OM2 as a result of major erosional truncation of up to 1000 m during the early stages of the Messinian Salinity Crisis (Kirkham et al., 2017) (Figs. 4, 5A and 5B). This erosional truncation resulted in a large number of ridges comprising remnants of OM2 which are now overlain exclusively by the Messinian Evaporites. In addition, the Base Salt surface is punctuated by several hundred circular to elliptical depressions that represent the depletion zones for mud volcanoes that erupted from the Pliocene to Recent (Fig. 5A, C & 5D). These are described in detail in Section 4.3.

The Messinian Evaporites are divided into an Upper Evaporitic Unit and a Lower Evaporitic Unit based on contrast in seismic facies. The Upper Evaporitic Unit is dominated by a transparent seismic facies that is typical of halite, whilst the Lower Evaporitic Unit comprises high amplitude and discontinuous reflections that are interbedded with seismically transparent layers (Fig. 4). These intra-salt reflections have been interpreted as thin clastic layers sourced from the Nile that were interbedded with salt precipitated during the Messinian Salinity Crisis (Kirkham et al., 2020a).

The Post Salt comprises a range of seismic facies and architectures that are typical of the slope succession of the Nile Deep Sea Fan (Loncke et al., 2004; Garziglia et al., 2008). These represent an assemblage of hemipelagites, with localised slope channel and levee systems and mass transport deposits (Fig. 4). Approximately 400 mud volcanoes have been identified and mapped within the Post Salt succession in the study area, and are interbedded within or extruded upon the background slope deposits. These are described in detail in the following section.

#### 4.2. Seismic expression of the Pliocene to Recent mud volcanoes

The Pliocene to Recent mud volcanoes are widely distributed throughout the study area (Kirkham et al., 2017). The best imaged and least deformed mud volcanoes are those that erupted in the Late Pleistocene to Recent (Fig. 6A). Older, more deeply buried mud volcanoes have been deformed by growth faulting, compaction and local subsidence associated with younger overlapping mud volcano systems. Hence their original geometry is more challenging to visualise and interpret (Fig. 6B).

Individual mud volcanoes are all defined as identifiable singular edifices by discrete and mappable upper and lower bounding surfaces that in all cases converge into a single reflection at their lateral margins (Figs. 4 and 6). There are no examples where the flanks of the edifices are seen to interfinger with the background sediments as is commonly described elsewhere (Deville et al. 2003, 2006). This implies that each



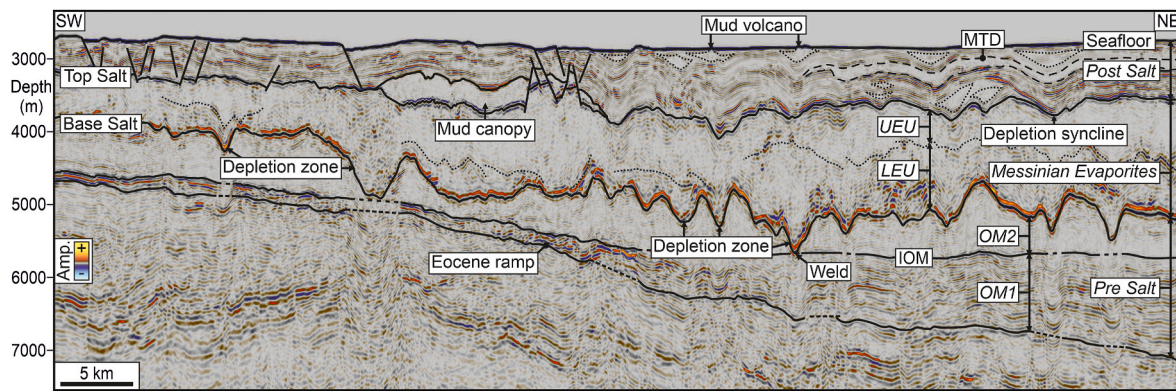


**Fig. 4.** A regional seismic cross-section in depth through the entire 3D seismic survey area (see Fig. 5A for location) showing the key marker horizons and stratigraphic units, as well as mud volcanoes and depletion zones. IOM – Intra-Oligo-Miocene; OM – Oligo-Miocene; UEU – Upper Evaporitic Unit; LEU – Lower Evaporitic Unit; MTD – Mass transport deposit.

edifice was emplaced in a sufficiently short time interval such that any background sediments accumulating in that interval are too thin to be resolved by the seismic data.

The recently erupted edifices give more representative values for maximum thickness and diameter, and there is a crude scaling between these two parameters (Kirkham et al., 2017). These younger edifices are all thickest in their centres directly above the position of the underlying conduit, with maximum thicknesses ranging from 20 m to 510 m (see Supplementary Table S1). Their diameters range from 550 m to 5660 m. The conduits are generally obvious on the seismic data, as trails of amplitude anomalies or discontinuities in the background reflectivity of the Post-Salt (Fig. 6A) and have been previously described in detail by Kirkham et al. (2018a, 2018b). The upper terminus of the majority of these conduits is a crater expressed at the basal surface with 10s–100s of metres of erosional relief, that forms part of the base to the overlying edifice (Fig. 6A) (Pryce et al., 2023). Thus, the initial extruded material typically fills the crater relief before building new seafloor topography.

The gross geometry of the basal surface of the majority of the recently erupted mud volcanoes is a bowl-shaped depression reminiscent of those observed previously to form the base of youthful mud volcanoes elsewhere (Fig. 6) (Camerlenghi et al., 1995; Robertson and Kopf, 1998; Kopf, 2002; Praeg et al., 2009). This grossly bowl-shaped morphology is typically seen to be mimicked on underlying layers throughout the entire Post Salt interval to the Top Salt with a remarkably consistent curvature and structural relief (Fig. 6). This crudely columnar, region represented by downward sagging beneath mud volcanoes has previously been interpreted as being the result of withdrawal of material at depth (Kirkham et al., 2017; Dupuis et al., 2019). Dupuis et al. (2019) suggested that these structures be regarded as a category of forced fold and noted that they could be seen as the inverse of forced domal folds formed by laccolithic or sill intrusions. For ease of description, we therefore refer to these structures as ‘depletion synclines’ and restrict our use of this term to structures that fulfil the criteria of being formed by depletion. In planform, these depletion synclines are commonly circular to elliptical, but more complex geometries are also observed where mud volcanoes are closely spaced (Fig. 5C & D).

The upper surface of the mud edifices is generally conical, but with a range of average flank angles from 0.2 to 15° and seafloor relief typically of a few 10s of meters up to 150 m (Fig. 7). The gross geometry of the mud edifices varies depending on the degree of curvature at the base, the amount of erosional relief of the basal crater, and the amount of surface relief built by the cumulative extrusive activity. The volumes of the recent edifices range from c. 0.1–3.3 km<sup>3</sup> (Supplementary Table S1).

Many mud volcanoes that have previously been described from seismic data elsewhere lack any internal stratification, and this has typically been attributed to the chaotic nature of the mud breccias comprising the bulk of the extruded products (Robertson and Kopf,

1998; Praeg et al., 2009). In marked contrast, the mud volcanoes in our study area exhibit a huge variety of internal reflection configurations and offer the potential to link the internal stratification to the characteristics of extrusion and contemporary subsidence (Fig. 7). These internal reflections are generally low to moderate amplitude, variable polarity and are grouped into two dominant seismic facies: (1) stratified, continuous with convergent onlap towards the margins, or (2) discontinuous to chaotic and mounded, commonly with a basal downlap (Fig. 7). We interpret the stratified facies as being the product of low viscosity slurry mud flows (c.f. Deville et al., 2006). The steep sided mounded geometries composed of discontinuous or chaotic facies are interpreted as resulting from much higher viscosity flows, probably consisting of mud breccias (by analogy with Deville et al., 2006).

Analysis of the internal configuration of 107 recently constructed edifices revealed the following general observations:

1. In the majority of edifices, the construction of a steep sided cone centred on the conduit is the initial stage in edifice construction, and later stages are marked by gentler dipping convergent onlapping units, that onlap the outer flank of the subsiding depression (e.g. Fig. 7A and D).
2. The majority of edifices exhibit an axio-symmetric fill geometry centred on the conduit, that is similar in any orientation of cross-section through the conduit. Only a small minority exhibit asymmetric fill geometry (e.g. Fig. 7D).
3. A minority exhibit an alternation of downlapping conical fills with stratified onlapping fill types.
4. A minority consist almost entirely of the stratified seismic facies, and exhibit classic centripetal convergent onlap towards the outer flanks.
5. Parallel onlap fill configurations are rarely observed.
6. Early downlap geometries at the bases of steep sided cones become progressively rotated into pseudo onlapping configurations by the later subsidence (e.g. Fig. 7D).
7. Underfilled geometries are observed where later stratified seismic facies onlap the unfilled space created by subsidence.
8. No examples of overfilling were observed: these would be recognisable where mud extruded beyond the margins of the subsiding area.
9. No examples of caldera type collapse structures were observed for any of the mud volcanoes. The only faults that affect edifice geometry are tectonic faults that form part of the margin-parallel growth fault array.

These observations collectively point to a filling regime where the extrusion of material precedes the subsidence that is commensurate with the mobilisation of that material at depth. Underfilling is only observed where the extruded volume forms a steeper sided cone, and the rotation of the basal downlap signifies the broader diameter region of subsidence



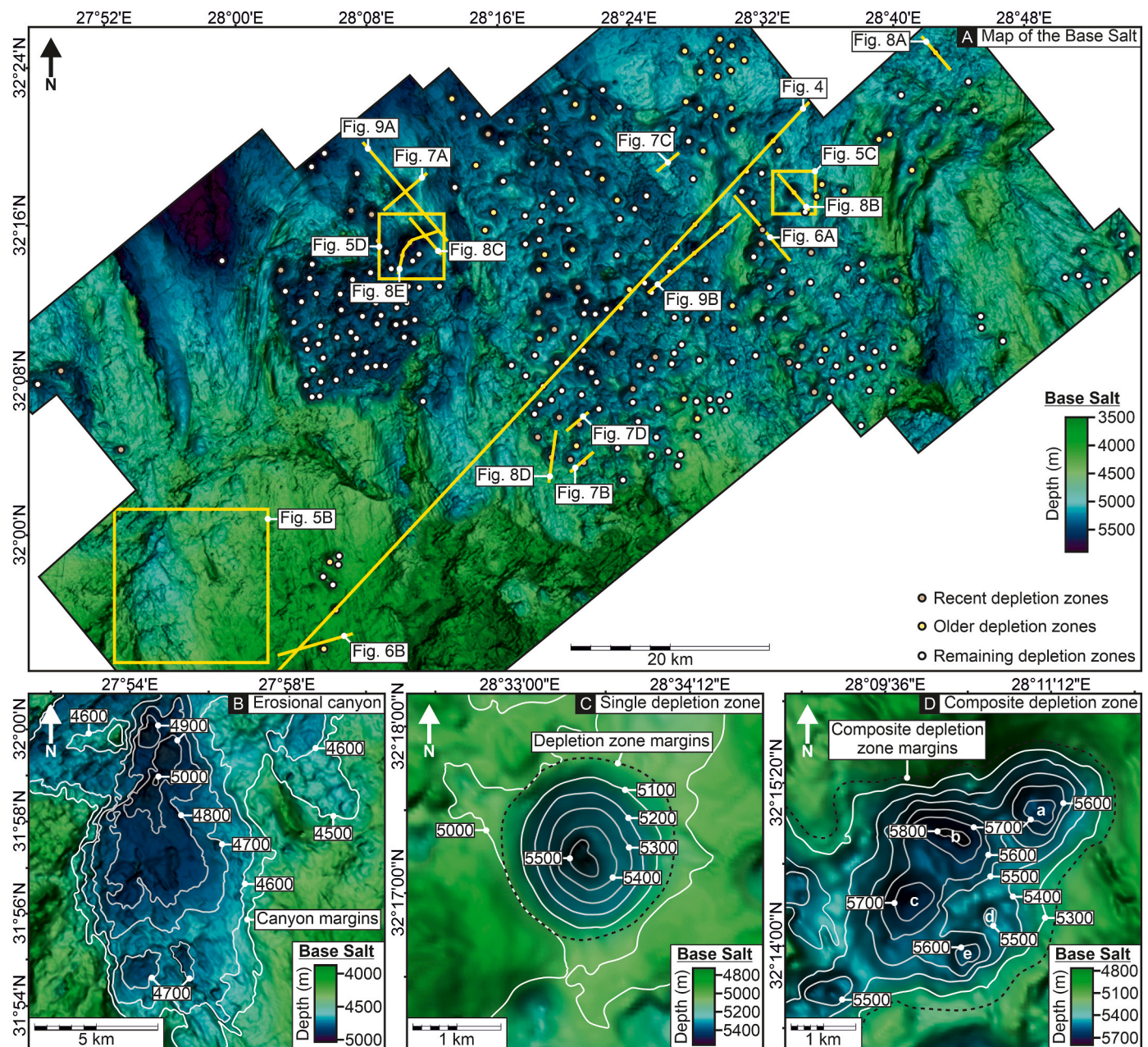


**Fig. 5.** Palaeogeomorphology of the Base Salt in the 3D seismic survey area. **A:** A depth map of the Base Salt in the 3D seismic survey area (see Fig. 2A for location) showing localised depressions (shown in more detail in Fig. 5B–D) and the location of 277 depletion zones. **B:** A depth map (see Fig. 5A for location) showing an erosional canyon at the Base Salt. **C:** A depth map (see Fig. 5A for location) showing a single depletion zone at the Base Salt. **D:** A depth map (see Fig. 5A for location) showing a composite depletion zone at the Base Salt that is composed of several (labelled a–e) closely spaced and overlapping depletion zones whose formation was diachronous.

catching up with this initial volumetric transfer to the surface. The reason for this lag between extrusion and subsidence is explored in the Discussion.

#### 4.3. Seismic expression of depletion zones

The depletion zones in the study area have been interpreted using a combination of two key criteria (Kirkham et al., 2017): (1) mapping circular or elliptical depressions at the Base Salt (Fig. 5), and (2) identifying a discrete and systematic thinning of a specific stratigraphic unit within the Pre Salt that corresponds to the mapped area of the depression at the Base Salt (Fig. 8). Kirkham et al. (2017) previously argued that the specific unit that has experienced mobilisation and removal to

form the depletion zone is restricted to OM2, directly beneath the Messinian Evaporites, and hence the Base Salt forms the base of the collapsed ‘roof’ stratigraphy (the depletion syncline) whose collective deformation is by subsidence into the space created by the removal of the mobilised volume (Dupuis et al., 2019).

Importantly, beneath larger depletion zones, various artefacts linked to the processing of the PSDM volume give the impression of a more deeply penetrating collapse structure involving OM1 (Fig. 8B & C). However, it is found that beneath smaller depletion zones, the reflections within the well imaged OM1 interval cross beneath the zone with no thickness variation or disruption whatsoever (Fig. 8A & D). This argues strongly in support of Kirkham et al. (2017) that OM2 acted as the parent or source layer, with no downward extension of the



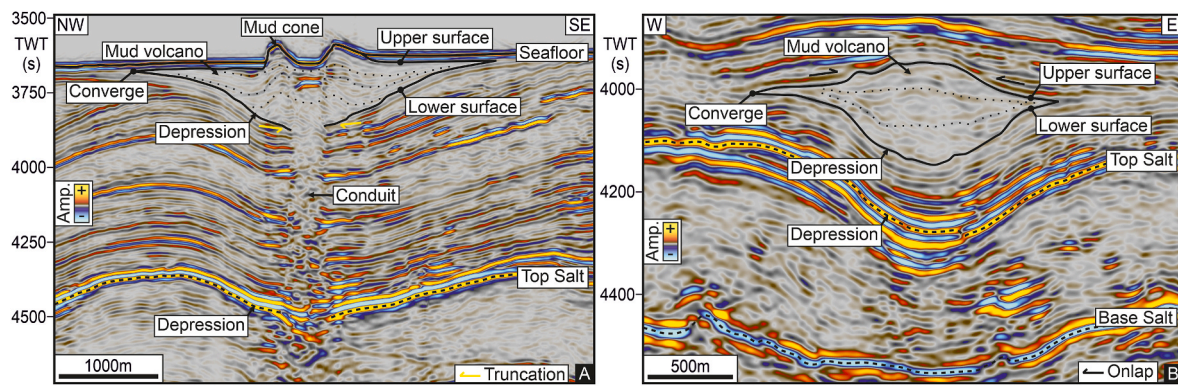


**Fig. 6.** Recently erupted and older mud volcanoes (see Fig. 5A for locations). **A:** A seismic cross-section in Two-Way-Time (TWT) showing a recently erupted mud volcano with a mud cone that crops at the present-day seafloor and is fed by a conduit. The Pliocene-Recent stratigraphy underlying the mud volcano has a depressed geometry. **B:** A seismic cross-section in Two-Way-Time (TWT) through an older mud volcano that is Pliocene in age. The underlying Pliocene-Recent stratigraphy has a depressed geometry.

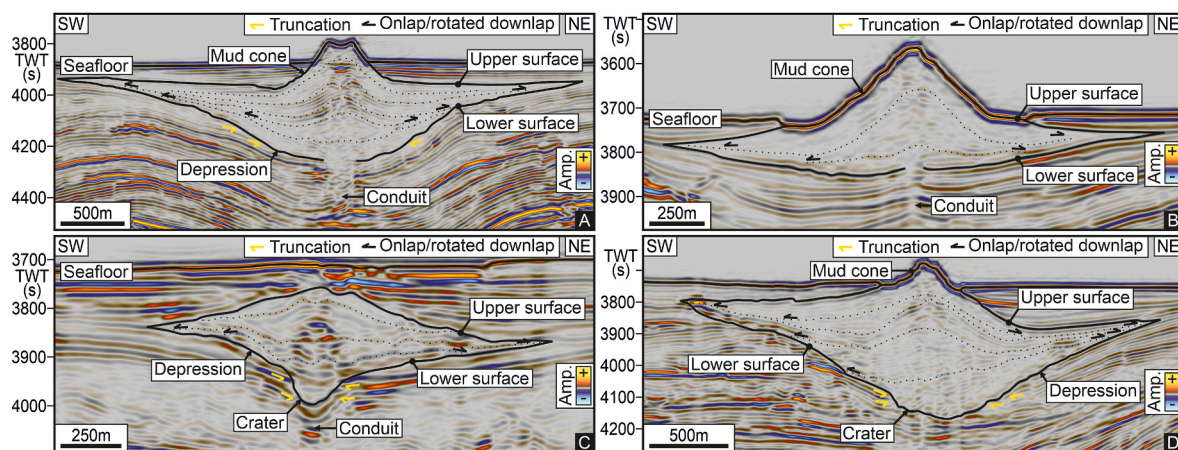


**Fig. 7.** The internal seismic stratigraphy of mud volcanoes in the study area from Two-Way-Time (TWT) cross-sections (see Fig. 5A for locations). The mud volcanoes display an upper and a lower surface onto which internal reflection show an onlap/rotated downlap relationship (A–D). Their internal reflections display a combination of conical, converging, stratified and parallel fill (A–D) that is predominantly axio-symmetric (A) or more rarely asymmetric (D). A conduit underlies many of these mud volcanoes (A, B & C). Some display erosional relief at their lower surface from a basal crater (C & D).

withdrawal of material into OM1.

Using these criteria, 86 relatively isolated depletion zones have been identified in the study area (Fig. 5), and of these 33 correspond to recently erupted mud volcanoes. Many additional depletion zones are recognised but have amalgamated with neighbouring depletion zones to form composite depletion zones (e.g. Fig. 5D & 8E), and these are not considered further here because they are too complex in form to provide reliable morphometric data. The following sections describe the morphometric data obtained from this large suite of depletion zones. Since they all derive from the same stratigraphic interval (OM2), this large dataset provides an opportunity to make process inferences from the quantitative analysis of the morphometric data.

#### 4.3.1. 3D geometry

Single isolated depletion zones are characterised by a circular to moderately elliptical depression at the Base Salt (Fig. 9). In cross section, the geometry at Base Salt can be symmetric or asymmetric, with a gently curved (Fig. 9B) or more conical shape (Fig. 9A). The imaging of the Base Salt in the PSDM seismic volume is sufficiently good as to distinguish these two end member types (see Supplementary Table S2 & Supplementary Fig. 1). However, the imaging is not able to resolve small discontinuities such as scarps or minor fault offsets at the Base Salt, and the mapped surfaces are therefore relatively smooth.

The outer margins of the depletion zones are typically marked by a

distinctive monoclinial hinge in the Base Salt, similar to the peripheral hinges described by Dupuis et al. (2019), from depletion zones offshore Nigeria. The inclined flanks of the depletion zones at Base Salt are planar to gently curved, but there is typically a central portion that maintains a constant dip, and these dip values were recorded relative to the datum of the base of the OM2 unit (Fig. 3 and see Methods).

These mid flank angles were measured for 87 depletion zones and their distribution is presented in Fig. 10A. They range from 11° to 41° with a crudely normal distribution, a median value of 26° and mean value of 25.5° (N = 344) (Supplementary Tables S2 and S3). These flank angles are discussed below in the context of the genesis of the depletion zone. For asymmetric forms, the ranges between the steepest and shallowest flanks are typically of the order of 10°. There is no systematic variation between the recently erupted subset of 33 depletion zones, versus the remainder. There is also no systematic variation of flank angle with depletion zone dimensions (Fig. 10B & C).

Diameters were measured between their peripheral hinges for the total population of 86 depletion zones, along with their structural relief, measured from a pre-depletion datum reconstructed at the Base Salt (see Methods). Long and short axis diameter measurements were obtained for all non-circular planforms (Supplementary Table S2) (Fig. 11). The range of maximum diameters is 790 m–3160 m, and the range of structural relief values is 100 m–730 m (Supplementary Table S3). Cross plots of maximum diameter versus relief show a moderate positive



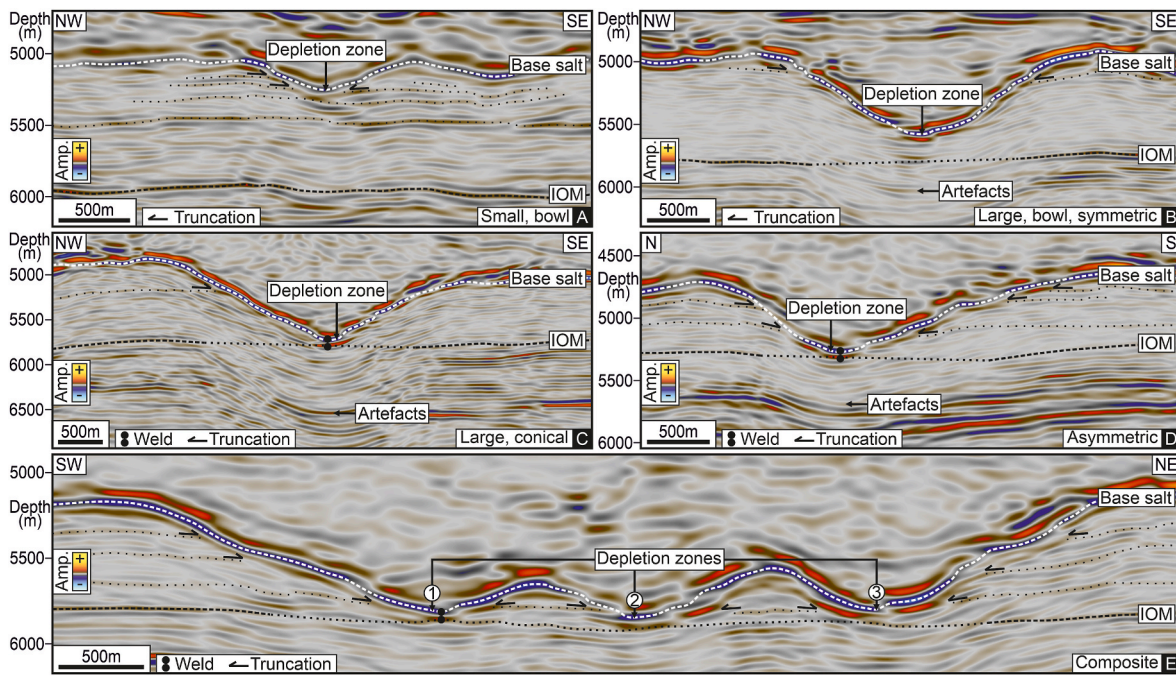


**Fig. 8.** Seismic character of depletion zones (see Fig. 5A for locations; seismic cross-sections are in depth). **A:** A seismic cross-section through a small bowl-shaped depletion zone. Reflections in OM2 terminate against the Base Salt. **B:** A seismic cross-section through a large depletion zone that is bowl-shaped, symmetric and is underlain by a vertical region of seismic artefacts. **C:** A seismic cross-section through a large and conical depletion zone. OM2 has been entirely removed creating a weld between the Base Salt and the IOM. **D:** A seismic cross-section through an asymmetric depletion zone that also exhibits a weld between the Base Salt and IOM. **E:** A seismic cross-section through part of a composite depletion zone that is composed here of three (1–3) individual depletion zones. The reflections of OM2 terminate against the Base Salt and depletion zone 1 shows a weld in this profile.

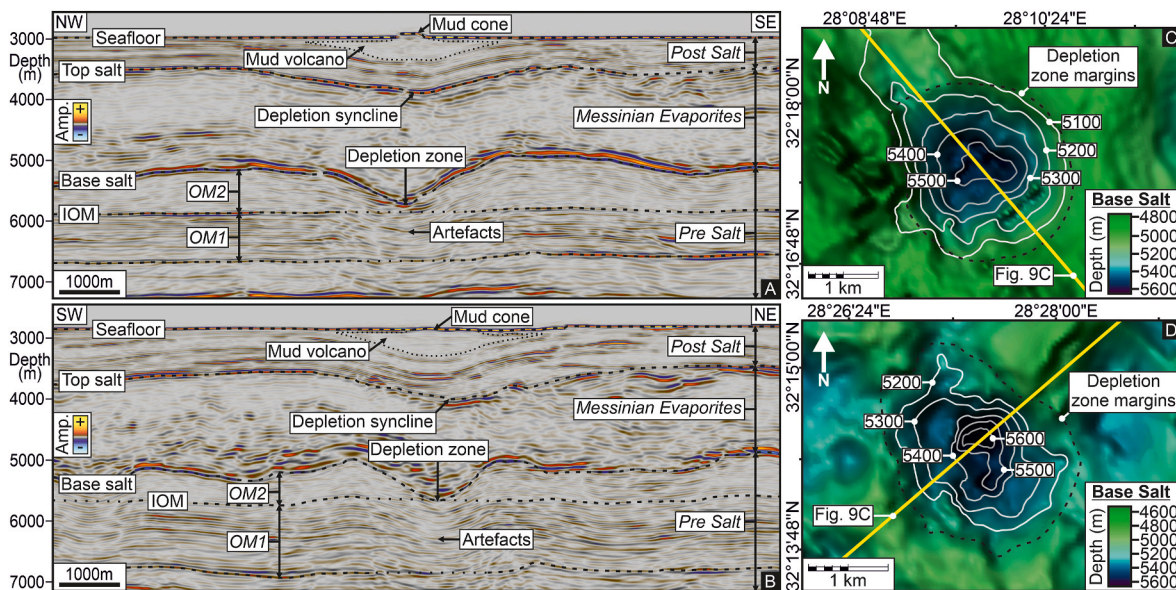


**Fig. 9.** The 3D geometry of depletion zones. **A & B:** Seismic profiles (see Fig. 9C & D for locations) in depth through depletion zones that are directly overlain by recently erupted mud volcano. The depletion zones show a depression at the Base Salt and localised thinning of OM2 that is underlain by parallel and continuous reflection of OM1. **C & D:** Depth maps of the Base Salt (see Fig. 5A for locations) from Fig. 9A & B showing the localised depressions of the depletion zones. The depletion zone in C is sub-axisymmetric and circular and the depletion zone in D is more asymmetric and irregular.

correlation coefficient ( $R^2 = 0.44$ ), that is interpreted to show a modest scaling relationship between relief and diameter (Fig. 11).

#### 4.3.2. Stratal geometry of the depletion zones

Seismic imaging of the reflection geometry in the Pre-Salt around and below the depletion zones is hampered by velocity and migration artefacts (Fig. 9A & B). The geometrical relationship between the

reflections in OM2 and the margins of depression at the Base Salt is particularly hard to categorise because of transmission and mode conversion artefacts generated by the steep dips of the Base Salt, and the large impedance contrast between the Messinian Evaporites and the fine-grained sediments of OM2. Hence, we cannot specify the precise geometrical relationship of the low to moderate amplitude reflections at the Base Salt across each depletion zone. However, for the smaller

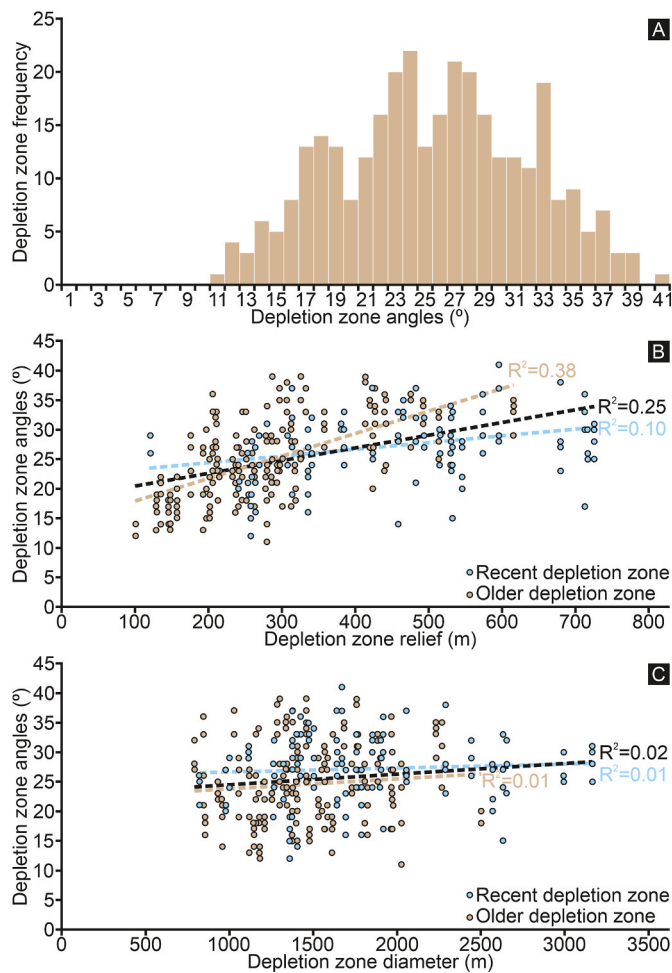


**Fig. 10.** Depletion zone slope angles. **A:** A histogram of 321 measured slope angles from a set of 86 depletion zones. **B:** A scatter chart of depletion zone angles vs. depletion zone relief. **C:** A scatter chart of depletion zone angles vs. depletion zone diameter. The data points in **B** & **C** are divided into angle measurements from recent depletion zones (Pleistocene–Recent; 120 angle measurements; light blue) and older depletion zones (201 angle measurements; light brown).  $R^2$  values are given for recent and older depletion zones, as well as all (black line).

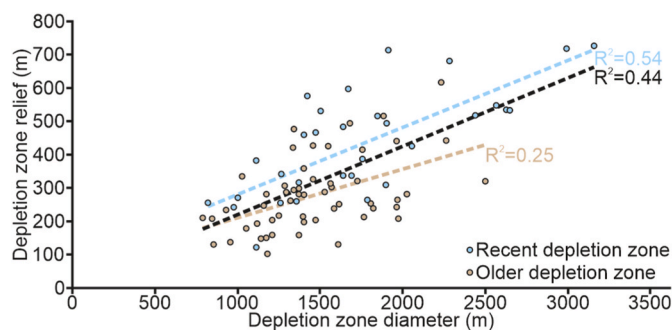


**Fig. 11.** A scatter chart of depletion zone relief vs. long axis diameter for a set of 86 depletion zones. The depletion zone data points are divided into recent depletion zones (Pleistocene–Recent; 33 depletion zones; light blue) and older depletion zones (53 depletion zones; light brown).  $R^2$  values are given for recent and older depletion zones, as well as all (black line).

depletion zones, the lower part of OM2 is undeformed across the depletion zone, suggesting that the contact geometry is truncational, rather than convergent (see Fig. 8A & E).

Importantly, none of the largest depletion zones appear to remove material from OM1. In 10 out of the 33 examples of recently erupted mud volcanoes, the deepest part of the depletion zone in each case is close to or just above the projected position of the IOM (e.g. Fig. 8C–E & 9), suggesting that the largest of the recently formed depletion zones have reached a limiting position where, within measurable limits the Base Salt is directly juxtaposed with the uppermost reflections of OM1. This type of configuration where a depleted parent unit is effectively completely removed from its subsurface position was termed a mud weld by Dupuis et al. (2019). The observation of putative welding at the IOM is therefore consistent with the earlier interpretation of Kirkham et al. (2017) that the parent unit is exclusively OM2.

#### 4.3.3. Geometry of the depletion synclines

Of the 33 recently erupted mud volcanoes, 22 are underlain by well-defined and isolated depletion synclines from which morphometric data can be recorded (e.g. Figs. 4, 6A and 9). The other 11 examples are underlain by depletion synclines that have been augmented by other closely adjacent depletion synclines or salt tectonic deformation and are too complex to extract accurate morphometric data. In the 22 measured examples of depletion synclines, the hinge-to-hinge distance in the Post Salt is significantly broader than the diameter of their respective underlying depletion zones (Figs. 4, 6A and 9). The structural relief of the depletion synclines within the Post Salt is less than the relief of the depletion zone in every measured case, typically by a factor of two. In all 22 cases, the thickness of the Messinian Evaporites measured above the deepest point of the depletion zone is greater than that in the region immediately surrounding the depletion zone in question (Fig. 12). These thickness changes imply that there must be local redistribution of the Messinian Evaporites to accommodate the formation of the depletion structure at the Base Salt. This compensating flow also explains the observed difference in the geometry of the depletion zone and the depletion syncline, with the latter having a systematically wider region of subsidence than would be perhaps expected from a simple vertical subsidence by collapse of the overburden to the depletion zone. This ‘depletion-induced salt flow’ would most probably have been concentrated in the deepest part of the Messinian Evaporites, within the reflective Lower Evaporite Unit (Fig. 9), but the entire unit must have been involved in the flow to some extent to account for the geometry of the Top Salt. The effect of this depletion-induced salt flow was therefore to broaden the zone of subsidence above the depletion zone and to reduce its magnitude to conserve the volume. Importantly, these observations imply that the depletion process is concurrent with salt flow, since the geometry of the surface depression at the base of the mud volcano is related to the geometry of the depletion syncline, and this is determined by the salt flow response to the underlying removal of material.

Of the 22 recently erupted mud volcanoes in the dataset, 10 were found to be suitable for volume balancing (Fig. 13). The volumes of the measured depletion zones, are within 20% of the volume of their respective mud volcanoes (Fig. 13). There is no systematic difference in the two volumes: half of the cases have larger mud volcano volume than depletion zone volumes, and vice versa. This suggests a significant measurement error is involved in the latter measurement, to compound any differences related to loss of pore fluid. Volume balancing of depletion zones and their eruptive equivalents has only been attempted on a few previous occasions, so this dataset of 10 depletion zones and their complementary mud volcanoes considerably extends the cumulative database to date.

## 5. Discussion

### 5.1. Source of the extruded material

The depletion zones described from the study area are an intrinsic component of the prolific mud volcanism that commenced in the early



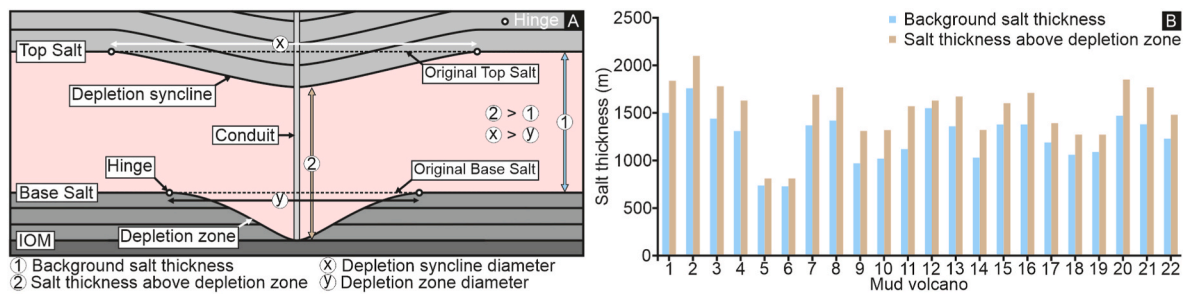


**Fig. 12.** Background salt thickness vs salt thickness above depletion zones. **A:** A schematic profile through a depletion zone, highlighting a greater salt thickness overlying a depletion zone (2) than the background salt thickness (1) and a depletion syncline (x) that is wider than the depletion zone (y). **B:** A bar chart showing the salt thickness above a set of 22 depletion zones (light brown) vs the adjacent background salt thickness (light blue). The thickness of the salt always increases overlying the depletion zone.

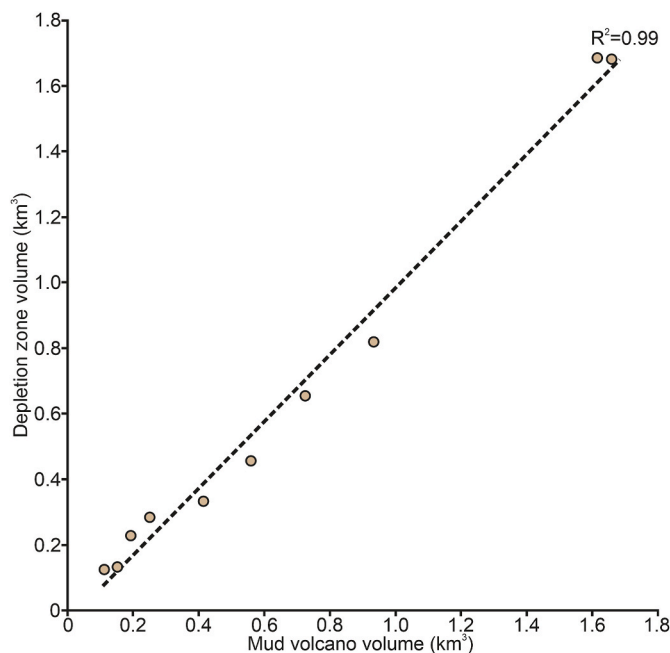


**Fig. 13.** A scatter chart showing the calculated volume of a set of 10 recently erupted depletion zones versus the calculated volumes of their associated mud volcanoes.

Pliocene and continues at the present day. By identifying layers with systematic truncation into these depletion zones, we argue that it was exclusively the slope deposits of Miocene age (OM2) that were mobilised and extruded (Figs. 8 and 9). The close correspondence of the extruded and depleted volumes (Fig. 13) is also most easily rationalised with what is essentially a single layer depletion model.

It has not been possible to completely rule out the involvement of deeper sourced fluids, but the absence of any obvious structures to act as a focus for pressure build up to the critical level needed to hydraulically fracture upwards over 2500 m to the surface argues against any primary involvement. The channelised and lobate submarine fan sandstones of OM1 are the most obvious aquifer that could have supplied fluids upwards, but the seismic data shows that this wedge-shaped unit is largely unstructured, and dips homoclinally basinwards (Fig. 4).

Recently, Kirkham et al. (2022) mapped several hundred fluid escape pipes and small ( $<0.01 \text{ km}^3$ ) mud cones in the study area that are not coupled to depletion zones in the Pre Salt. These fluid escape pipes were shown to emanate from the crest of erosional stratigraphic traps of OM2 at the Base Salt. The combination of three-dimensional seal configuration and low permeability of the Messinian Evaporites would have provided an ideal template for the development of overpressures high

enough to induce hydraulic fracturing and fluid escape.

By analogy, we suggest that similar stratigraphic traps would have provided loci for high overpressure to develop in OM2, thus fostering the conditions necessary for mud mobilisation. We suggest that mud mobilisation first initiated at the crest of stratigraphic traps at the Base Salt, most likely with expulsion of high-pressure pore fluid and methane forming craters at the seafloor (Pryce et al., 2023) and the depletion zones evolved from there, modifying the geometry of the Base Salt as depletion proceeded. Thus a single source layer is a simple explanation for the fluid and solid components of all the mud volcanism in the area. This source layer (OM2) contained in its initial conditions (fluid composition and pressure, lithology, diagenetic state) the necessary ingredients to yield a muddy slurry for upwards transport to build the edifices above the salt.

## 5.2. Episodicity in the eruptive history

Alternations of relatively high and low viscosity components expressed in the internal stratification of the mud volcanoes (Fig. 7) accounts for the variety of the seismic facies stacking patterns within individual mud volcanoes and also points to variability or episodicity in the processes generating the muddy slurries at depth. The variation in topographic relief and flank angles of mud volcanoes has previously been linked to slurry viscosity (Kopf, 2002), and it has been suggested that viscosity variation may be due to clast content, pore fluid or gas content, or to the original water content of the parent material (Kopf et al., 2005). Without direct calibration of the mud volcanoes in the study area, we can only suggest that the variation is most likely to be due to variation within the parent unit at depth, rather than from sampling within the conduits, simply due to the approximate mass balancing between depletion zones and edifices (Fig. 13).

## 5.3. Subsidence of depletion synclines moderated by salt flow

The contrast in geometry of the depletion zones (deeper relief and narrower), compared to depletion synclines (shallower relief and wider) was suggested above to be due to the ability of the salt to flow to fill the space vacated by mud mobilisation and extrusion. What then are the relative time scales of depletion versus induced salt flow?

We have no direct means of measuring the duration of extrusion involved in any single mud volcano in the study area. Taking estimates of extrusion rate provided by Kopf and Behrmann (2000) for mud volcanoes on the nearby Mediterranean Ridge, the typical edifice volume of  $0.5 \text{ km}^3$  could have been extruded in  $<100$  years. This estimate is also consistent with our observation that the edifices all converge to a single reflection at the margins. This extrusion rate is faster than the typical flow rate of salt that might be expected for a typical viscosity of  $10^{18} \text{ Pa s}$  (Jackson and Hudec, 2017). For comparison the flow rate of diapir crests or closure rates of excavated salt caverns are comparable and of the order of 1–15 mm/year. However, a more precise estimate of the flow



rate would require modelling with appropriate boundary conditions. On balance, we suggest that it is likely that the extrusion rate exceeded the response flow rate of the salt. This means that any initial depletion volume in OM2 might not immediately be filled by the flowing salt, and a mud filled chamber would most likely persist at the locus of depletion until such time as the salt flow could respond to replace the mobilised volume.

This faster relative rate of extrusion compared to induced salt flow rate also implies that the surface subsidence resulting from depletion would lag behind the extrusion of mud at surface. Evidence for this time lag can be seen in many of the mud volcanoes where the initial eruption consists of the more viscous slurry comprising a conical mound with a basal downlap (e.g. Fig. 7B). In these cases, a moat like area developed around the mound as the broader subsiding region created more accommodation space, and this moat was subsequently overlapped by later, less viscous flows.

#### 5.4. Mobilisation mechanism

Having established that the locus of sediment mobilisation required to feed the mud volcanoes was in the single parent layer of OM2, we now discuss if the well imaged morphology of the depletion zones in the study area provides any clues as to the precise nature of the mobilisation process and whether any inferences be made regarding the evolution of the depletion zones.

Previous evaluations of the sediment mobilisation involved in mud volcanism have largely invoked fluidization as the primary mechanism (Yassir, 1989; Brown, 1990; Kopf, 2002). Fluidization is widely defined as a liquifying mechanism in which sediment strength is lost through drag forces buoyantly balancing or exceeding the particle weight (Lowe, 1975; Maltman and Bolton, 2003). In the case of mud volcanism, the upward flow of pore fluid and/or gas is seen as the main driver, where the flow velocity provides the necessary lift for the transport of the solid fraction (Brown, 1990; Kopf and Behrmann, 2000). Some form of fracture or open conduit flow must therefore be invoked for fluidization to

occur on the necessary scale to provide the extruded volumes since the flow velocity in the conduit is most likely to exceed the fluidization velocity for small particle size (Kopf and Behrmann, 2000). The common occurrence of clasts in mud breccias erupted at surface requires conduits with centimetre to metre scale openings (Kopf, 2002), and apertures of this scale are consistent with high enough flow velocities to suspend mud slurry particles and clasts.

Whereas fluidization can be envisaged to occur as a form of wallrock abrasion or collapse from the margins and roof of conduits, it is harder to accept that it could wholly account for larger volumetric mobilisation from regions more distant from the conduit. The velocity of pore fluid or gas (e.g. methane) flowing towards the open conduit from within the main body of the source layer is dictated by the permeability, and is likely to be of the order of metres/year (Bjørlykke, 2006), far too low to lead to large volume disaggregation of cohesive, muddy sediments. Unless there are open fracture pathways throughout the source layer, it therefore seems unlikely that fluidization could mobilise the source unit for any substantial distance (>10 s m) away from the conduit. In the study area, the lack of any obvious focused flow pathways from aquifers beneath OM2 (Kirkham et al., 2022) is a further impediment to the possible involvement of fluidization via a through-going conduit transecting the mud source layer.

Kirkham et al. (2017) and Dupuis et al. (2019) both favoured mobilisation mechanisms based on liquefaction in order to solve this specific problem (Fig. 14). Liquefaction in this context can be differentiated from fluidization in that it applies to a process whereby sediment strength is lost by the pore fluid pressure taking on the full overburden load, such that effective stress goes to zero (Maltman and Bolton, 2003). Kirkham et al. (2017) suggested that pressure build up in the source unit would lead to liquefaction of an initial small volume, and removal of this volume would lead to further liquefaction in the surrounding volume. A cyclic process of liquefaction by this means was suggested to result in the propagation of a liquefaction front through the source layer from a central locus, and extraction of the mobilised volume could lead in turn to roof collapse and a positive feedback with overpressuring of the

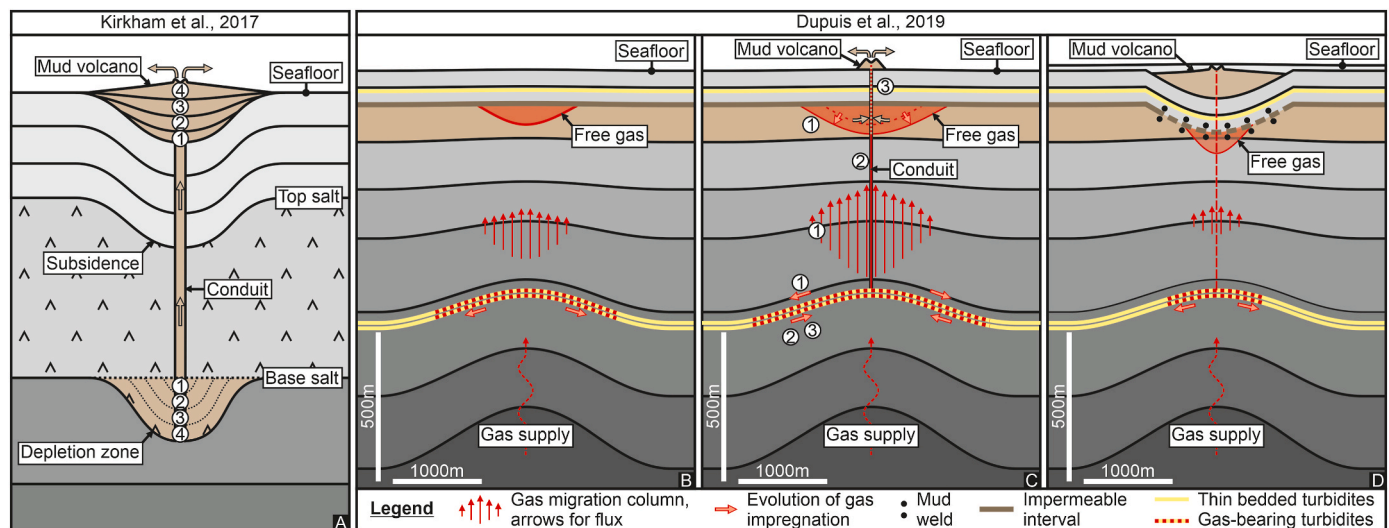


**Fig. 14.** Existing models for single layer liquefaction and depletion (modified from the original figures). **A:** Kirkham et al. (2017) model for dynamic liquefaction during the formation of a depletion zone, offshore Egypt. The model presents 4 cycles of liquefaction of a highly overpressure source layer, mud remobilisation, extrusion at the surface and subsidence and collapse of the overburden that triggers the next episode in the cycle. The depletion zone evolves radially downwards and outward from where the conduit roots to the Base Salt. **B-D:** Dupuis et al. (2019) model for the evolution of a mud volcano system offshore Nigeria. **B:** The upward migration of deeply sourced gas charges a thin bedded reservoir (turbidites). This reservoir leaks, leading to an overlying gas migration column and accumulation of a free gas lens in fine grained sediments beneath a shallower impermeable interval. **C:** Increased and laterally expansive gas flux (1) lead to hydraulic fracturing of the top seal of the reservoir and fluid leakage (2), a decrease in the gas column and a pressure reduction in the free gas-bearing lens. Pressure is further reduced when the hydraulic fractures reach the seafloor, causing gas expansion in the environs of the hydraulic fractures. These trigger (3) remobilisation of the fine-grained and free gas-bearing lens and radial growth of the depletion zone. **D:** The process is cyclical, with gas recharge and vertical downbuilding of the depletion zone to an eventual mud weld.

source layer (Fig. 14A).

Dupuis et al. (2019) also invoked a cyclic process whereby deeper gas migration led to the threshold pressure for hydraulic fracturing of the overburden above a gas saturated source layer. They argued that the propagation of the hydraulic fractures to the surface led to a pressure drop at the base of the fracture network and the resultant gas exsolution within this source layer provided the mechanism for liquefaction (Fig. 14B–D). Gas exsolution within muddy sediments has been invoked previously to explain subsurface mobilisation (Riis et al., 2005; Lawrence and Cartwright, 2010; Imbert et al., 2014) and there is strong experimental support that this process is an efficient means of developing a muddy slurry from an initially cohesive muddy sediment under a confining load (Pralle et al., 2003; Sultan et al., 2012; Blouin et al., 2019).

### 5.5. Implications of depletion zone geometry for the mobilisation process

The morphometric data from our study area provide strong support for the mud volcanism in the area having been fuelled by liquefaction rather than fluidization. The strong correlation between depth and diameter for the larger data set (recently erupted and older mud volcanoes) implies that depletion zones widen as they deepen (Fig. 11). Since the immediate roof to the depletion zone is the Messinian Evaporites, this correlation further suggests that the depletion process nucleated at the interface between OM2 and the base of the Messinian Evaporites, and enlargement was by a top-down process as suggested by Kirkham et al. (2017) and Dupuis et al. (2019).

This ‘top-down’ propagation model explains the observation that for the smallest depletion zones (diameters of <1 km, relief of <100 m), there is no evidence of thinning of underlying strata within OM2. We argue that the development of depletion zones can be viewed as a continuum process in which the smaller depletion zones can be regarded as immature forms, that for some reason did not evolve further by deepening and widening. Hence their restriction to the uppermost part of OM2 implies that the growth of depletion zones migrates downwards into progressively older layers.

In a ‘top down’ model of remobilisation by progressive liquefaction of a single source layer, there would be an ultimate limit to growth of the depletion zone once the base of this layer is intersected by the liquefaction front, and the result would be a mud weld (Dupuis et al., 2019). The largest group of depletion zones all touch down to a mud weld at the top of OM1 (Figs. 4, 8C–E, 9 A & 9 B). OM1 most likely contains a large fraction of coarse facies as evidenced by channelised and lobate seismic facies (Kellner et al., 2018; Kirkham et al., 2022), and this suggests that the downward liquefaction process was not capable of mobilising a stratigraphic unit with a higher coarse fraction. This may be entirely lithological, or because of pore fluid pressure variation resulting from the presence of coarser facies.

The most striking observation that the morphometric data provide, however, is the normal distribution of the flank angles of the depletion zones about mean and median values of 26° (Fig. 10A). The lack of correlation between flank angle and depth or diameter implies that immature forms evolve into mature forms with a similar range of flank angles implying a self-similar growth process. When combined with the critical observation that the contact at the lateral margins of the depletion zone is truncational (Fig. 8A & E), this suggests that the mobilisation of the parent sediment is a laterally propagating failure mechanism that cuts back retrogressively into the virgin unit as the depletion zone grows.

How might this retrogressive mobilisation process operate, and what factors would control the ultimate geometry of this type of depletion zone? The detailed processes involved within and around the depletion zone are unknown, and poorly constrained by direct observation. By inference, from observations of the final morphology, combined with constraints from surface sampling and the internal configuration of the mud volcanoes, it is possible to propose a sequence of events that have

certain physical boundary conditions, that might be a starting point for more rigorous testing with numerical modelling. We envisage that initial extraction of a small volume of pore fluid and methane at the immediate base of the newly formed conduit would change the stress state in the immediately surrounding region of the source layer (OM2) such that shear failure would occur. The fluid pressure in OM2 required to form the initial hydraulic fractures through the salt is close to or even slightly greater than the lithostatic pressure because the differential stress in the salt is assumed to be low (1–2 MPa) whilst the tensile strength could be up to 6 MPa as an upper bound (Kirkham et al., 2022). This implies that the effective stress within OM2 just below the salt is close to zero. As such, these sediments are highly susceptible to liquefaction, and a small stress or pressure perturbation might be sufficient to destabilise these already weak sediments.

Once liquefaction initiates at the root of the conduit, a small volume of muddy slurry bears the full overburden load, at the interface of OM2 and the salt, and the pressure gradient drives this slurry up the conduit to erupt an initial flow at the surface. The slurry pressure must be at or close to lithostatic, and must be maintained above the closure pressure of the hydraulic fractures in the conduit throughout the eruptive life span of the mud volcano (Fig. 15). Given this high slurry fluid pressure, the effective stress at the interface between the intact OM2 and the liquefied slurry is expected to be near zero with pressure applied perpendicular to the depletion surface (static fluids cannot apply shear stress) as long as the slurry flows up the conduit. When pressure decays and the slurry recovers some strength, delayed roof collapse into the slurry-filled chamber would help to induce further failure of the intact OM2 sections which would fail progressively in a top-down manner to adapt to the subsiding roof. We envisage that intact OM2 sediment is mobilised by the process of undrained-contraction loading (Schofield and Wroth, 1968; Santamarina et al., 2001), or to use an alternative term, shear-induced liquefaction (c.f. Maltman and Bolton, 2003; Soto et al., 2021). Continuous removal of the slurry via the open conduit would lead to a pressure drop in the remaining slurry volume (which may be cyclic) and provide the necessary loss of lateral support to induce failure of the intact section of OM2, thus accounting for the self-similar growth history and the upper limit in the observed flank angles (Fig. 10A).

The specific physical properties of OM2 are likely to have played a critical role in predisposing this unit to liquefy (Maltman and Bolton, 2003). Important parameters could include the methane saturation (Sultan et al., 2012; Imbert et al., 2014; Blouin et al., 2019), the salinity of the pore fluids and their impact on inter-particle cohesion (Santamarina et al., 2001), or grain size and grain mineralogy (Bull et al., 2009). Unfortunately, with no direct borehole calibration of these physical properties and a relative lack of surface sampling of the muds at the few active mud volcanoes in the area (Giresse et al., 2010), it is difficult to assess the role specific parameters may have played.

### 5.6. Proposed model for depletion zone evolution

Based on the preceding discussion and incorporating elements of both Kirkham et al. (2017) and Dupuis et al. (2019), we suggest the following evolutionary model for the depletion zones in the study area (Fig. 15).

#### A. Seal failure

Pressure builds within OM2 from an already high Pre Salt overpressure resulting from the events associated with the Messinian Salinity Crisis (Kirkham et al., 2022). Possible sources of additional overpressure could be hydrocarbon buoyancy, biogenic gas generation or other diagenetically induced pressure increases (e.g. osmotic pressure). There is no evidence for active tectonic compression in this area, so we can exclude tectonic overpressuring and also rapid sedimentation as possible contributory sources of overpressure. The pressure foci were crestal

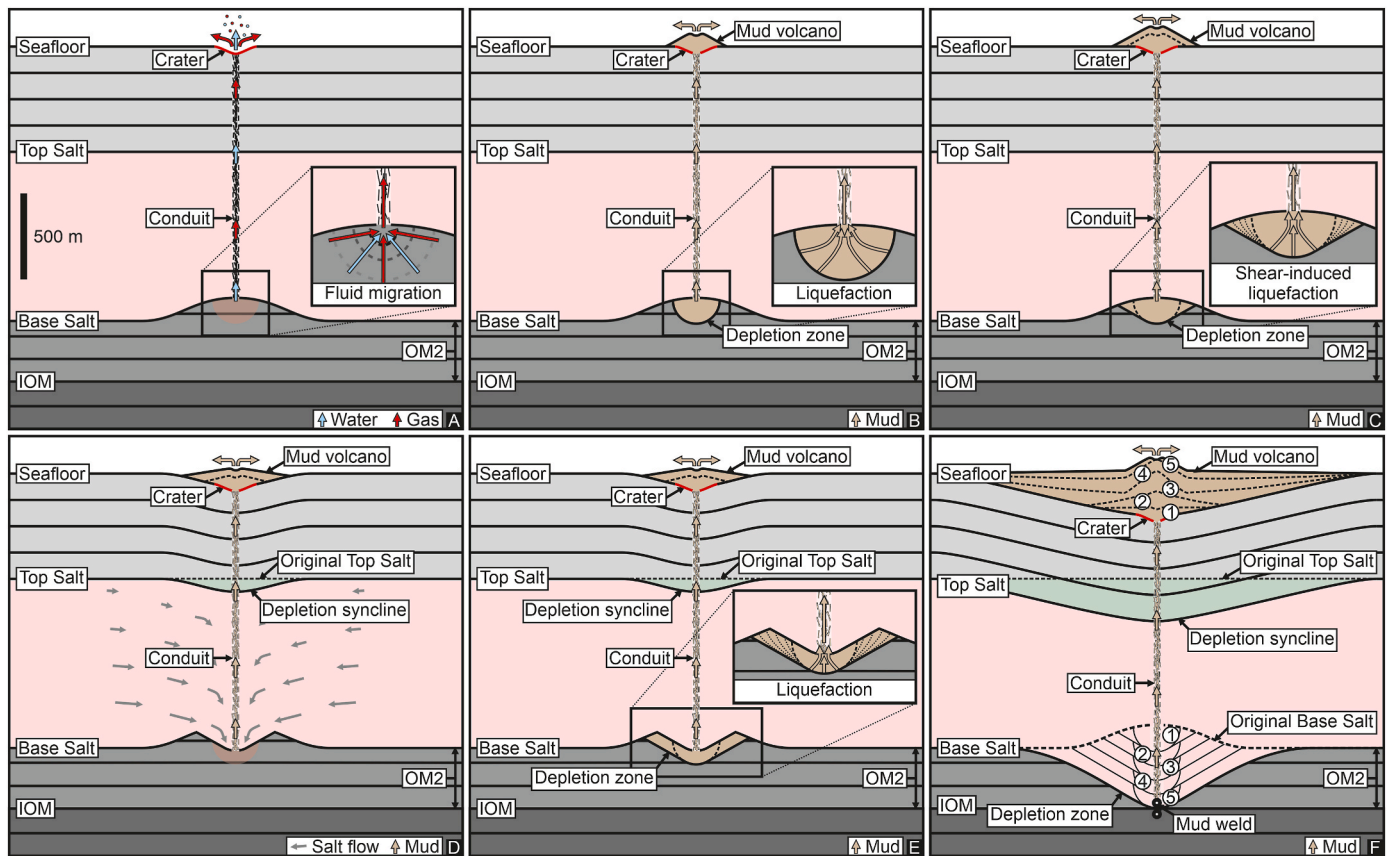


**Fig. 15.** A schematic model for depletion zone evolution (see text for detailed description of stages A-F). **A:** Pressure builds in a stratigraphic trap at the Base Salt until a critical threshold for hydraulic fracturing is reached. Vertical scale bar is approximate and representative for the study area. **B:** The flux of pore fluids and gas into the hydraulic fractures destabilises the sediments at the base conduit, triggering localised liquefaction and the formation of an initial depletion zone. **C:** The drainage of mud slurry causes a pressure drop in the depletion zone that leads to progressive shear-induced liquefaction that propagates outwards to a stable slope. **D:** The mud slurry pressure drops, the roof of the depletion zone (Base Salt) collapses by salt flow into the depleted region. **E:** Re-pressurisation at the top seal interface triggers a new phase of liquefaction and the deepening and widening of the depletion zone at the base of the conduit. **F:** This cyclical process continues until a mud weld is formed.

regions of stratigraphic traps formed by erosion during the Messinian Salinity Crisis (Fig. 15A). The pressure would continue to build until it reaches the fracture pressure gradient, which is the threshold value for hydraulic failure of the evaporite seal (Kirkham et al. 2018a, 2018b; 2022). Since over 400 mud volcanoes formed in this area, it is likely that the threshold pressure was achieved on a local, rather than regional basis, and there was limited pressure communication within OM2.

Hydraulic fractures propagate to the surface, crossing the > 1 km thick Messinian Evaporites and the Post Salt, transporting an initial fluid-dominated flux of pore fluid and gas extracted from the immediate vicinity of the leak point of the evaporite seal. The hydraulic fractures coalesce into a pipe-like conduit consisting of a fracture network (Kirkham et al. 2018a, 2018b). In the majority of cases, this initial flux was sufficient to excavate craters at the fluid venting site at the seafloor with gas expansion as the fluid column ascends close to the venting site providing a major driver for the excavation of near-surface sediments (Fig. 15A) (Pryce et al., 2023).

#### B. Initial eruption

At the base of the conduit, the influx of pore fluid and gas into the hydraulic fracture network destabilises a region of OM2 with a very low effective stress resulting in localised liquefaction of OM2. The details of this initial liquefaction are unknown, but this may possibly involve gas exsolution or expansion as suggested by Dupuis et al. (2019), or inward wall collapse at the base of the hydraulic fractures, analogous to

borehole collapse in underbalanced drilling of highly overpressured shales. The initially mobilised sediment volume is transported to the surface to form mounds within the pockmark craters (Fig. 15B).

#### C. Roof collapse and propagation of the liquefaction front

The removal of the initially mobilised sediment from the growing depletion zone creates the conditions for further growth (Fig. 15C). As muddy slurry is transported up the fracture network to form the initial eruptive flows and is drained from the depletion zone, the pressure of the remaining slurry drops, leading to a zone of shear failure and collapse of intact OM2 propagating retrogressively radially outwards as a liquefaction front from the central locus. The margins of the collapsed region are akin to a failure scarp, controlled by the bulk internal friction of the layer that is being mobilised (c.f. Bull et al., 2009).

The fracture network is maintained as an open conduit as long as the muddy slurry occupying the depletion zone has a pressure greater than the fracture closure pressure (equal to the minimum stress, Hubbert and Willis, 1957). The slurry pressure must oppose the horizontal confining stress within the salt acting to close the fracture walls and seal off the conduit. Any viscous pressure losses during upward ascent of the slurry may well be compensated by pressure and density changes resulting from expansion of gas bubbles within the slurry (Collignon et al., 2017). Some dissolution of the salt may occur and would act to widen the fracture conduits, reduce roughness, and increase flow velocity (Dupré et al., 2014).



#### D. Temporary hiatus in eruptive activity

As the slurry pressure drops during further extraction of slurry up the conduit, the roof would begin to collapse by salt flow, squeezing out residual slurry into the conduit, to the point where any further extrusion up the conduit is inhibited or blocked (Fig. 15D). The viscosity of the slurry mobilised into the conduit would vary depending on the physical properties of the section of intact OM2 that is being mobilised (c.f. Kopf et al., 2005). The flow of slurry into the conduit would be limited by any support for the salt roof provided by the fluid pressure of the liquefied volume. We follow Dupuis et al.'s (2019) suggestion that roof collapse may therefore control the volume of any initial eruption. If the pressure drops below the closure pressure, the conduit may close and seal before the roof collapse has fully evacuated the slurry volume.

#### E. Resumption of Activity.

A hiatus would follow until pressure builds again at the top seal interface (the base of the conduit), sufficiently to reactivate the fracture network or to form a new set of hydraulic fractures across the salt. Once again, a localised slurry filled region may form at the base of the conduit (Fig. 15E), and this acts to deepen the depletion zone. The collapse of the margins of this mud chamber in turn triggers a new stage of radial propagation of the liquefaction front, and the transport of the slurry to the conduit results in a deeper and wider depletion zone, again with a flank angle controlled by the internal friction of the layer being mobilised. We note that the time scale of any cyclicity is unknown, but short interruptions in the extrusion of mud flows are strongly suggested by the internal reflection geometries of the mud volcanoes (Fig. 7).

#### F. Termination of Activity.

Activity may be terminated by the development of a mud weld at any interface between the source layer (or sub-layer) and an underlying unit that for reasons of lithology, diagenesis or pore pressure is not susceptible to dynamic liquefaction (Fig. 15F). Activity may also be terminated or skewed asymmetrically if the lateral migration of the liquefaction front encounters an obstacle to liquefaction, or if the pressure drops in the conduit beneath the fracture closure pressure. There is evidently a lateral limit to the distance the depletion zone can expand radially from the conduit. In the study area this amounts to about a kilometre. This may be related to the interplay between the strength of the salt and its ability to support the overburden load and the pressure distribution in the slurry filled depletion zone. Numerical modelling of this limit to lateral extent would be invaluable to further evaluate the reasons for this lateral limit.

#### 5.7. Wider implications of the model

The model as proposed above is based heavily on only two areas (Offshore Egypt and Nigeria) where 3D seismic has been used as the main medium with which to identify and describe depletion zones. As such it relies on specific stratigraphic and structural factors contributing to the formation of mud volcanoes in these two areas. Nevertheless, the fundamental attributes of the model may be much more widely applicable. The vast majority of studies of mud volcanism that have considered the source of the mud and the mobilisation mechanism have concluded that multiple source layers have provided fluids and solid components. However, in the specific case of the West Nile mud volcano province, we follow Kirkham et al. (2017) and Dupuis et al. (2019) in invoking a process of single layer mobilisation and depletion, where the in-situ conditions of the source layer predispose it to liquefaction. We suggest that liquefaction during shear failure has the potential to be a more efficient means of mobilising large subsurface volumes of muddy sediments than fluidization, and may provide an alternative explanation for the wide, bowl shaped regions of subsidence observed at the surface

associated with many other mud volcanoes world-wide (Camerlenghi et al., 1995; Dimitrov, 2002; Praeg et al., 2009; Deville et al., 2010; Mazzini and Etiope, 2017). As we have shown, the width of the zone of surface subsidence does not necessarily match the subsurface dimensions of the depletion zone, but in many cases should be of the same order, and are therefore typically an order of magnitude larger than conduit diameters. This alone makes fluidization of conduit walls a less likely explanation for the geometry of the surface subsidence depressions.

The model also has the advantage in only requiring critical conditions for liquefaction to be met in a single layer, as opposed to a multi-source layer. Highly overpressured source layers are common in many areas of rapid burial, hydrocarbon generation or tectonic compression (Osborne and Swarbrick, 1997; Li et al., 2022), and these tend to be the common factors involved in mud volcanism (Kopf, 2002; Mazzini and Etiope, 2017). We suggest therefore that single layer depletion by liquefaction may be much more widely responsible for mud volcanism than in the limited number of cases reported to date.

## 6. Conclusions

Depletion zones associated with hundreds of small mud volcanoes erupted at intervals from the early Pliocene to Recent on the western part of the Nile Cone are recognisable on 3D seismic data from their characteristic circular to elliptical planform, narrow range of dimensions (c. 1–2 km diameter), and anomalous patterns of thinning in the units undergoing remobilisation and transport to the surface. The source layer for this impressive array of mud volcanoes is shown to be a single unit, of probably Mid- Late Miocene age, referred to as OM2. The depletion zones exhibit characteristic bowl or cone shapes (concave upwards), with flank angles that have a remarkably narrow range of dips. 312 flank angle measurements were made from 86 depletion zones, of which 22 were formed recently. The data are normally distributed with mean flank angles of 26°. A model for the depletion zones is developed whereby overpressure build up in OM2 at stratigraphic traps leads to hydraulic fracturing across >1000 m thick evaporite succession, fluid venting, and mobilisation of the source layer of mud by shear-induced liquefaction.

## Declaration of competing interest

The authors declare that they have no known competing financial interests or personal relationships that could have appeared to influence the work reported in this paper.

## Data availability

The data that has been used is confidential.

## Acknowledgments

We would like to thank Equinor (Stavanger, Norway) for provision of the 3D seismic data and Schlumberger for providing academic licences for their seismic interpretation software, Petrel. We thank Richard Katz, Christopher MacMinn and Luke Kearney for valuable discussions and feedback on an earlier draft of the manuscript. This research did not receive any specific grant from funding agencies in the public, commercial, or not-for-profit sectors. DNE is grateful for financial support from Texas Global Faculty Research Seed Grants. We thank editor Davide Oppo and reviewer Chris Morley for constructive feedback during the review process.

## Appendix A. Supplementary data

Supplementary data to this article can be found online at <https://doi.org/10.1016/j.marpetgeo.2023.106351>.

## References

- Aal, A.A., El Barkooky, A., Gerrits, M., Meyer, H., Schwander, M., Zaki, H., 2000. Tectonic evolution of the eastern mediterranean basin and its significance for hydrocarbon prospectivity in the ultradeepwater of the Nile delta. *Lead. Edge* 19, 1086–1102. <https://doi.org/10.1190/1.1438485>.
- Abd El-Fattah, B.K., Moustafa, A.R., Yousef, M., 2021. A new insight into the structural evolution of Rosetta Fault, eastern margin of Herodotus Basin, East Mediterranean. *Mar. Petrol. Geol.* 131, 105161 <https://doi.org/10.1016/j.marpetgeo.2021.105161>.
- Allen, H., Jackson, C.A.-L., Fraser, A.J., 2016. Gravity-driven deformation of a youthful saline giant: the interplay between gliding and spreading in the Messinian basins of the Eastern Mediterranean. *Petrol. Geosci.* 22, 340–356. <https://doi.org/10.1144/petgeo2016-034>.
- Bjørlykke, K., 2006. Effects of compaction processes on stresses, faults, and fluid flow in sedimentary basins: examples from the Norwegian margin. *Geol. Soc. Lond., Spec. Pub.* 253, 359–379. <https://doi.org/10.1144/GSL.SP.2006.253.01.19>.
- Blouin, A., Sultan, N., Callot, J.P., Imbert, P., 2019. Sediment damage caused by gas exsolution: a key mechanism for mud volcano formation. *Eng. Geol.* 263, 105313 <https://doi.org/10.1016/j.enggeo.2019.105313>.
- Brown, A.R., 2004. Interpretation of Three-Dimensional Seismic Data. American Association of Petroleum Geologists Tulsa, pp. 31–60. <https://doi.org/10.1190/1.9781560802884.ch2>.
- Brown, K.M., 1990. The nature and hydrogeologic significance of mud diapirs and diatremes for accretionary systems. *J. Geophys. Res. Solid Earth* 95, 8969–8982. <https://doi.org/10.1029/JB095iB06p08969>.
- Bull, S., Cartwright, J., Huuse, M., 2009. A subsurface evacuation model for submarine slope failure. *Basin Res.* 21, 433–443. <https://doi.org/10.1111/j.1365-2117.2008.00390.x>.
- Camerlenghi, A., Cita, M.B., Vedova, B.D., Fusi, N., Mirabile, L., Pellis, G., 1995. Geophysical evidence of mud diapirism on the Mediterranean Ridge accretionary complex. *Mar. Geophys. Res.* 17, 115–141. <https://doi.org/10.1007/BF01203423>.
- Cita, M.B., 1981. Prometheus mud breccia: an example of shale diapirism in the western Mediterranean ridge. *Annales géologiques des Pays helléniques* 30, 543–570.
- Collignon, M., Mazzini, A., Schmid, D.W., Lupi, M., 2017. Modelling fluid flow in active clastic piercements: challenges and approaches. *Mar. Petrol. Geol.* 90, 157–172. <https://doi.org/10.1016/j.marpetgeo.2017.09.033>.
- Davies, R.J., Brumm, M., Manga, M., Rubiandini, R., Swarbrick, R., Tingay, M., 2008. The East Java mud volcano (2006 to present): an earthquake or drilling trigger? *Earth Planet. Sci. Lett.* 272, 627–638. <https://doi.org/10.1016/j.epsl.2008.05.029>.
- Deville, E., Battani, A., Griboulard, R., Guerlais, S., Herbin, J.P., Houzay, J.P., Muller, C., Prinzhofer, A., 2003. The origin and processes of mud volcanism: new insights from Trinidad. *Geol. Soc. Lond., Spec. Pub.* 216, 475–490. <https://doi.org/10.1144/GSL.SP.2003.216.01.31>.
- Deville, E., Guerlais, S.H., Callec, Y., Griboulard, R., Huyghe, P., Lallemand, S., Mascle, A., Noble, M., Schmitz, J., Collaboration of the Caramba Working Group, 2006. Liquefied vs stratified sediment mobilization processes: insight from the South of the Barbados accretionary prism. *Tectonophysics* 428, 33–47. <https://doi.org/10.1016/j.tecto.2006.08.011>.
- Deville, E., Guerlais, S.-H., 2009. Cyclic activity of mud volcanoes: evidences from Trinidad (SE Caribbean). *Mar. Petrol. Geol.* 26, 1681–1691. <https://doi.org/10.1016/j.marpetgeo.2009.03.002>.
- Deville, E., Guerlais, S.H., Lallemand, S., Schneider, F., 2010. Fluid dynamics and subsurface sediment mobilization processes: an overview from Southeast Caribbean. *Basin Res.* 22, 361–379. <https://doi.org/10.1111/j.1365-2117.2010.00474.x>.
- Dimitrov, L.I., 2002. Mud volcanoes—the most important pathway for degassing deeply buried sediments. *Earth Sci. Rev.* 59, 49–76. [https://doi.org/10.1016/S0012-8252\(02\)00069-7](https://doi.org/10.1016/S0012-8252(02)00069-7).
- Dolson, J., 2020. The petroleum geology of Egypt and history of exploration. In: Hamimi, Z., El-Barkooky, A., Martínez Frías, J., Fritz, H., Abd El-Rahman, Y. (Eds.), *The Geology of Egypt*, 635–658. Regional Geology Reviews, the Geology of Egypt. Springer.
- Dolson, J., Boucher, P., Siok, J., Heppard, P., 2005. Key challenges to realizing full potential in an emerging giant gas province: Nile Delta/Mediterranean offshore, deep water, Egypt. In: Geological Society, London, Petroleum Geology Conference Series. Geological Society of London, pp. 607–624. <https://doi.org/10.1144/0060607>.
- Dupré, S., Mascle, J., Foucher, J.-P., Harmegnies, F., Woodside, J., Pierre, C., 2014. Warm brine lakes in craters of active mud volcanoes, Menes caldera off NW Egypt: evidence for deep-rooted thermogenic processes. *Geo Mar. Lett.* 34, 153–168. <https://doi.org/10.1007/s00367-014-0367-1>.
- Dupré, S., Woodside, J., Foucher, J.P., De Lange, G., Mascle, J., Boetius, A., Mastalerz, V., Stadnitskaia, A., Ondreas, H., Huguen, C., Harmegnies, F., 2007. Seafloor geological studies above active gas chimneys off Egypt (central Nile Deep Sea Fan). *Deep Sea Res. Oceanogr. Res. Pap.* 54 (7), 1146–1172. <https://doi.org/10.1016/j.dsr.2007.03.007>.
- Dupuis, M., Imbert, P., Odonne, F., Vendeville, B., 2019. Mud volcanism by repeated roof collapse: 3D architecture and evolution of a mud volcano cluster offshore Nigeria. *Mar. Petrol. Geol.* 110, 368–387. <https://doi.org/10.1016/j.marpetgeo.2019.07.033>.
- Etiopie, G., Klusman, R.W., 2002. Geologic emissions of methane to the atmosphere. *Chemosphere* 49, 777–789. [https://doi.org/10.1016/S0045-6535\(02\)00380-6](https://doi.org/10.1016/S0045-6535(02)00380-6).
- Fowler, S., Mildenhall, J., Zalova, S., Riley, G., Elsley, G., Desplanques, A., Guliyev, F., 2000. Mud volcanoes and structural development on Shah Deniz. *J. Petrol. Sci. Eng.* 28, 189–206. [https://doi.org/10.1016/S0920-4105\(00\)00078-4](https://doi.org/10.1016/S0920-4105(00)00078-4).
- García-Castellanos, D., Estrada, F., Jiménez-Munt, I., Gorini, C., Fernández, M., Vergés, J., De Vicente, R., 2009. Catastrophic flood of the Mediterranean after the Messinian salinity crisis. *Nature* 462, 778–781. <https://doi.org/10.1038/nature08555>.
- Garziglia, S., Migeon, S., Ducassou, E., Loncke, L., Mascle, J., 2008. Mass-transport deposits on the Rosetta province (NW Nile deep-sea turbidite system, Egyptian margin): characteristics, distribution, and potential causal processes. *Mar. Geol.* 250, 180–198. <https://doi.org/10.1016/j.marpetgeo.2008.01.016>.
- Giresse, P., Loncke, L., Huguen, C., Muller, C., Mascle, J., 2010. Nature and origin of sedimentary clasts associated with mud volcanoes in the Nile deep-sea fan. Relationships with fluid venting. *Sediment. Geol.* 228, 229–245. <https://doi.org/10.1016/j.sedgeo.2010.04.014>.
- Graue, K., 2000. Mud volcanoes in deepwater Nigeria. *Mar. Petrol. Geol.* 17, 959–974. [https://doi.org/10.1016/S0264-8172\(00\)00016-7](https://doi.org/10.1016/S0264-8172(00)00016-7).
- Hsu, K.J., Montadert, L., Bernoulli, D., Cita, M.B., Erickson, A., Garrison, R.E., Kidd, R.B., Mèlières, F., Müller, C., Wright, R., 1977. History of the Mediterranean salinity crisis. *Nature* 267, 399–403. <https://doi.org/10.1038/267399a0>.
- Hubbert, M.K., Willis, D.G., 1957. Mechanics of hydraulic fracturing. *Transact. Am. Inst. Mech. Eng.* 210, 153–168. <https://doi.org/10.2118/686-G>.
- Huguen, C., Foucher, J.-P., Mascle, J., Ondreas, H., Thouement, M., Gontharet, S., Stadnitskaia, A., Pierre, C., Bayon, G., Loncke, L., 2009. Menes caldera, a highly active site of brine seepage in the Eastern Mediterranean sea: “In situ” observations from the NAUTINIL expedition (2003). *Mar. Geol.* 261, 138–152. <https://doi.org/10.1016/j.marpetgeo.2009.02.005>.
- Imbert, P., Geiss, B., Fatjó de Martín, N., 2014. How to evacuate 10 km<sup>3</sup> of mud: saturate with gas and decrease the pressure. *Geo Mar. Lett.* 34, 199–213. <https://doi.org/10.1007/s00367-014-0357-3>.
- Jackson, M.P., Hudec, M.R., 2017. Salt Tectonics: Principles and Practice. Cambridge University Press, pp. 28–60. <https://doi.org/10.1017/9781139003988>.
- Kellner, A., Brink, G., El Khawaga, H., 2018. Depositional history of the western Nile delta, Egypt: late Rupelian to Pleistocene. *AAPG (Am. Assoc. Pet. Geol.) Bull.* 102, 1841–1865. <https://doi.org/10.1306/0216187234>.
- Kirkham, C., Cartwright, J., Hermanrud, C., Jebsen, C., 2017. The spatial, temporal and volumetric analysis of a large mud volcano province within the Eastern Mediterranean. *Mar. Petrol. Geol.* 81, 1–16. <https://doi.org/10.1016/j.marpetgeo.2016.12.026>.
- Kirkham, C., Cartwright, J., Hermanrud, C., Jebsen, C., 2018a. The formation of giant clastic extrusions at the end of the Messinian Salinity Crisis. *Earth Planet. Sci. Lett.* 482, 434–445. <https://doi.org/10.1016/j.epsl.2017.11.001>.
- Kirkham, C., Cartwright, J., Hermanrud, C., Jebsen, C., 2018b. The genesis of mud volcano conduits through thick evaporite sequences. *Basin Res.* 30, 217–236. <https://doi.org/10.1111/bre.12250>.
- Kirkham, C., Bertoni, C., Cartwright, J., Lensky, N.G., Sirota, I., Rodriguez, K., Hodgson, N., 2020a. The demise of a ‘salt giant’ driven by uplift and thermal dissolution. *Earth Planet. Sci. Lett.* 531, 115933 <https://doi.org/10.1016/j.epsl.2019.115933>.
- Kirkham, C., Cartwright, J., Bertoni, C., Van Rensbergen, P., 2020b. The genesis of a giant mud canopy by catastrophic failure of a thick evaporite sealing layer. *Geology* 48, 787–791. <https://doi.org/10.1130/G47430.1>.
- Kirkham, C., Cartwright, J., 2022. Mud volcanoes and dissolution structures as kinematic markers during salt tectonic deformation. *Basin Res.* 34, 99–120. <https://doi.org/10.1111/bre.12612>.
- Kirkham, C., Cartwright, J., James, D., Kearney, L., 2022. Episodic venting of extreme subsalt overpressure through a thick evaporitic seal. *Mar. Petrol. Geol.* 142, 105741 <https://doi.org/10.1016/j.marpetgeo.2022.105741>.
- Kopf, A., Behrmann, J.H., 2000. Extrusion dynamics of mud volcanoes on the Mediterranean Ridge accretionary complex. *Geol. Soc. Lond., Spec. Pub.* 174, 169–204. <https://doi.org/10.1144/GSL.SP.1999.174.01.10>.
- Kopf, A.J., 2002. Significance of mud volcanism. *Rev. Geophys.* 40 (2) <https://doi.org/10.1029/2000RG000093>, 2-1-2-52.
- Kopf, A.J., Clennell, M.B., Brown, K.M., 2005. Physical properties of muds extruded from mud volcanoes: implications for episodicity of eruptions and relationship to seismicity. In: *Mud Volcanoes, Geodynamics and Seismicity: Proceedings of the NATO Advanced Research Workshop on Mud Volcanism, Geodynamics and Seismicity Baku*. Springer Netherlands, pp. 263–283. [https://doi.org/10.1007/1-4020-3204-8\\_24](https://doi.org/10.1007/1-4020-3204-8_24). Azerbaijan 20–22 May 2003.
- Lawrence, G.W., Cartwright, J.A., 2010. The stratigraphic and geographic distribution of giant craters and remobilised sediment mounds on the mid Norway margin, and their relation to long term fluid flow. *Mar. Petrol. Geol.* 27, 733–747. <https://doi.org/10.1016/j.marpetgeo.2009.10.012>.
- Li, C., Zhan, L., Lu, H., 2022. Mechanisms for overpressure development in marine sediments. *J. Mar. Sci. Eng.* 10 (4), 490. <https://doi.org/10.3390/jmse10040490>.
- Loncke, L., Mascle, J., Parties, F.S., 2004. Mud volcanoes, gas chimneys, pockmarks and mounds in the Nile deep-sea fan (Eastern Mediterranean): geophysical evidences. *Mar. Petrol. Geol.* 21, 669–689. <https://doi.org/10.1016/j.marpetgeo.2004.02.004>.
- Loncke, L., Gaullier, V., Mascle, J., Vendeville, B., Camera, L., 2006. The Nile deep-sea fan: an example of interacting sedimentation, salt tectonics, and inherited subsalt paleotopographic features. *Mar. Petrol. Geol.* 23, 297–315. <https://doi.org/10.1016/j.marpetgeo.2006.01.001>.
- Lofi, J., Sage, F., Déverchère, J., Loncke, L., Maillard, A., Gaullier, V., Thion, I., Gillet, H., Guennoc, P., Gorini, C., 2011. Refining our knowledge of the Messinian salinity crisis records in the offshore domain through multi-site seismic analysis. *Bull. Soc. Geol. Fr.* 182, 163–180. <https://doi.org/10.2113/gssgfbull.182.2.163>.
- Lowe, D.R., 1975. Water escape structures in coarse-grained sediments. *Sedimentology* 22, 157–204. <https://doi.org/10.1111/j.1365-3091.1975.tb00290.x>.
- Maltman, A.J., Bolton, A., 2003. How Sediments Become Mobilized, vol. 216. Geological Society, London, Special Publications, pp. 9–20. <https://doi.org/10.1144/GSL.SP.2003.216.01.02>.

- Masclé, J., Mary, F., Praeg, D., Brosolo, L., Camera, L., Ceramicola, S., Dupré, S., 2014. Distribution and geological control of mud volcanoes and other fluid/free gas seepage features in the Mediterranean Sea and nearby Gulf of Cadiz. *Geo Mar. Lett.* 34, 89–110. <https://doi.org/10.1007/s00367-014-0356-4>.
- Mazzini, A., Etiope, G., 2017. Mud volcanism: an updated review. *Earth Sci. Rev.* 168, 81–112. <https://doi.org/10.1016/j.earscirev.2017.03.001>.
- Meilijson, A., Hilgen, F., Sepúlveda, J., Steinberg, J., Fairbank, V., Flecker, R., Waldmann, N.D., Spaulding, S.A., Bialik, O.M., Boudinot, F.G., 2019. Chronology with a pinch of salt: integrated stratigraphy of Messinian evaporites in the deep Eastern Mediterranean reveals long-lasting halite deposition during Atlantic connectivity. *Earth Sci. Rev.* 194, 374–398. <https://doi.org/10.1016/j.earscirev.2019.05.011>.
- Milkov, A., 2000. Worldwide distribution of submarine mud volcanoes and associated gas hydrates. *Mar. Geol.* 167, 29–42. [https://doi.org/10.1016/S0025-3227\(00\)00022-0](https://doi.org/10.1016/S0025-3227(00)00022-0).
- Mousoulotis, A., Albanakis, K., Georgakopoulos, A., Papatheodorou, G., Tripanas, E., Medvedev, B., 2020. Pre-salt clastic systems in the herodotus basin, SE Mediterranean Sea. *Mar. Petrol. Geol.* 122, 104691 <https://doi.org/10.1016/j.marpetgeo.2020.104691>.
- Netzeband, G., Hübscher, C., Gajewski, D., 2006. The structural evolution of the Messinian evaporites in the Levantine Basin. *Mar. Geol.* 230, 249–273. <https://doi.org/10.1016/j.marpetgeo.2006.05.004>.
- Osborne, M.J., Swarbrick, R.E., 1997. Mechanisms for generating overpressure in sedimentary basins: a reevaluation. *AAPG (Am. Assoc. Pet. Geol.) Bull.* 81, 1023–1041. <https://doi.org/10.1306/522B49C9-1727-11D7-8645000102C1865D>.
- Praeg, D., Ceramicola, S., Barbieri, R., Unnithan, V., Wardell, N., 2009. Tectonically-driven mud volcanism since the late Pliocene on the Calabrian accretionary prism, central Mediterranean Sea. *Mar. Petrol. Geol.* 26, 1849–1865. <https://doi.org/10.1016/j.marpetgeo.2009.03.008>.
- Planke, S., Svensen, H., Hovland, M., Banks, D.A., Jamtveit, B., 2003. Mud and fluid migration in active mud volcanoes in Azerbaijan. *Geo Mar. Lett.* 23, 258–268. <https://doi.org/10.1007/s00367-003-0152-z>.
- Pralle, N., Külzer, M., Gudehus, G., 2003. Experimental evidence on the role of gas in sediment liquefaction and mud volcanism. *Geol. Soc. Lond., Spec. Pub.* 216, 159–171. <https://doi.org/10.1144/GSL.SP.2003.216.01.11>.
- Pryce, E., Kirkham, C., Cartwright, J., 2023. Crater formation during the onset of mud volcanism. *Geology* 51, 252–256. <https://doi.org/10.1130/G50713.1>.
- Riis, F., Berg, K., Cartwright, J., Eidvin, T., Hansch, K., 2005. Formation of large, crater-like evacuation structures in ooze sediments in the Norwegian Sea. Possible implications for the development of the Storegga Slide. In: Ormen Lange–An Integrated Study for Safe Field Development in the Storegga Submarine Area. Elsevier, pp. 257–273. <https://doi.org/10.1016/B978-0-08-044694-3.50026-3>.
- Robertson, A.H., Kopf, A., 1998. Origin of clasts and matrix within the Milano and Napoli mud volcanoes, Mediterranean Ridge accretionary complex. *Proc. Ocean Drill. Progr. Sci. Results* 160 (Chapter 45).
- Ryan, W.B., 2009. Decoding the Mediterranean salinity crisis. *Sedimentology* 56, 95–136. <https://doi.org/10.1111/j.1365-3091.2008.01031.x>.
- Salem, R., 1976. Evolution of Eocene-Miocene sedimentation patterns in parts of northern Egypt. *AAPG (Am. Assoc. Pet. Geol.) Bull.* 60, 34–64. <https://doi.org/10.1306/83D92280-16C7-11D7-8645000102C1865D>.
- Santamarina, J.C., Klein, K.A., Fam, M.A., 2001. *Soils and Waves*. J. Wiley & Sons, New York, pp. 124–152.
- Schofield, A.N., Wroth, P., 1968. *Critical State Soil Mechanics*, vol. 310. McGraw-Hill, London, pp. 226–235.
- Soto, J.I., Heidari, M., Hudec, M.R., 2021. Proposal for a mechanical model of mobile shales. *Sci. Rep.* 11, 1–11. <https://doi.org/10.1038/s41598-021-02868-x>.
- Sultan, N., De Gennaro, V., Puech, A., 2012. Mechanical behaviour of gas-charged marine plastic sediments. *Geotechnique* 62, 751–766. <https://doi.org/10.1680/geot.12.OG.002>.
- Stewart, S.A., Davies, R.J., 2006. Structure and emplacement of mud volcano systems in the South Caspian Basin. *AAPG (Am. Assoc. Pet. Geol.) Bull.* 90, 771–786. <https://doi.org/10.1306/11220505045>.
- Underwood, C.J., King, C., Steurbaut, E., 2013. Eocene initiation of Nile drainage due to East African uplift. *Palaeogeogr. Palaeoclimatol. Palaeoecol.* 392, 138–145. <https://doi.org/10.1016/j.palaeo.2013.09.014>.
- Woodside, J., Masclé, J., Zitter, T., Limonov, A., Ergün, M., Volkonskaia, A., 2002. The Florence Rise, the western bend of the Cyprus arc. *Mar. Geol.* 185, 177–194. [https://doi.org/10.1016/S0025-3227\(02\)00194-9](https://doi.org/10.1016/S0025-3227(02)00194-9).
- Yassir, N.A., 1989. *Mud Volcanoes and the Behaviour of Overpressured Clays and Silts*. Doctoral dissertation, University of London.
- Zucker, E., Gvirtzman, Z., Steinberg, J., Enzel, Y., 2020. Salt tectonics in the Eastern Mediterranean Sea: where a giant delta meets a salt giant. *Geology* 48, 134–138. <https://doi.org/10.1130/G47031.1>.